An optical labeling-based proliferation assay system reveals the paracrine effect of interleukin-6 in breast cancer

Junji Itou[1*], Sunao Tanaka[1], Fumiaki Sato[1], Ryutaro Akiyama[2,3], Yasuhiko Kawakami[2,3,4,5] and Masakazu Toi[1]

1. Department of Breast Surgery, Graduate School of Medicine, Kyoto University, 54 Shogoin-Kawahara-cho, Sakyo-ku, Kyoto 606-8507, Japan

2. Department of Genetics, Cell Biology and Development, University of Minnesota, 321 Church Street SE, Minneapolis, MN55455, USA

3. Stem Cell Institute, University of Minnesota, 321 Church Street SE, Minneapolis, MN55455, USA

4. Developmental Biology Center, University of Minnesota, 321 Church Street SE, Minneapolis, MN55455, USA

5. Lillehei Heart Institute, University of Minnesota, 321 Church Street SE, Minneapolis, MN55455, USA

***Corresponding author:** Junji Itou

54 Shogoin-Kawahara-cho, Sakyo-ku, Kyoto 606-8507, Japan

Tel: +81-75-751-3660, Fax: +81-75-751-3616

e-mail: junji-itou@umin.ac.jp

Abstract

Proliferation analysis is one of the basic approaches to characterize various cell types. In conventional cell proliferation assays, the same sample cannot be observed over time, nor can a specific group within a heterogeneous population of cells, for example, cancerous cells, be analyzed separately. To overcome these limitations, we established an optical labeling-based proliferation assay system with the Kaede protein, whose fluorescence can be irreversibly photoconverted from green to red by irradiation. After a single non-toxic photoconversion event, the intensity of red fluorescence in each cell is reduced by cell division. From this, we developed a simple method to quantify cell proliferation by monitoring reduction of red fluorescence over time. This study shows that the optical labeling-based proliferation assay is a viable novel method to analyze cell proliferation, and could enhance our understanding of mechanisms regulating cell proliferation machinery. We used this newly established system to analyze the functions of secreted interleukin-6 (IL-6) in cancer cell proliferation, which had not been fully characterized. Reduction in proliferation was observed following IL-6 knockdown. However, after co-culturing with IL-6-expressing cells, the proliferation of Kaede-labeled IL-6-knockdown cells was restored. These data indicate that in basal-like breast cancer cells, IL-6 exhibits a paracrine effect to positively regulate cell proliferation. Our results thus demonstrate that cancer cells can secrete signaling molecules, such as IL-6, to support the proliferation of other cancer cells.

Highlights:

An optical labeling-based proliferation assay (the OPA system) has been established.

The OPA system allows continuous observation of the same culture.

The OPA system enables analysis of a specific group in co-culture experiments.

The OPA system reveals interleukin-6 can exhibit a paracrine effect.

Interleukin-6 promotes breast cancer cell proliferation in a paracrine manner.

Keywords: Breast cancer; Interleukin-6; Optical labeling; Paracrine effect; Proliferation; The OPA system

Abbreviations:

BrdU: bromodeoxyuridine

hpi: hours post-irradiation

IL-6: interleukin-6

MMC: mitomycin C

STAT3: signal transduction and activator of transcription 3

The OPA system: the optical labeling-based proliferation assay system

1. Introduction

The cell proliferation machinery orchestrates events including DNA replication, duplication of cellular components, disappearance of the nuclear membrane, chromosome segregation, reconstruction of the nuclear membrane and cytoplasmic division. Although a significant number of studies have identified various factors that regulate cell proliferation, we still have much to learn about how these processes are regulated, particularly in transformed cells.

Cancer cells are highly proliferative as a consequence of the up-regulation of cell cycle activators [1, 2], the activation of signaling pathways [1, 3], mutations in genes controlling the cell cycle [1, 4], genomic amplification [5], and epigenetic changes [6]. The majority of cancer cells actively proliferate in culture, cancer cell cultures are useful models for the study of cell proliferation.

Breast cancer cells develop in mammary microenvironments, arising from the mammary epithelium. However, molecular and cellular characteristics, including proliferative ability, vary among breast cancer cells [7, 8]. Breast cancers are classified into subtypes according to differences in the expression of various markers [9-11]. The existence of various types of breast cancer originating from an identical cellular background suggest that use of these cell lines can enable the study of a variety of potential mechanisms used to activate the proliferation machinery, without having to consider differences in cellular origin and environmental stimuli.

Conventional methods of analyzing cell proliferation can be grouped into three categories. The first method is counting the number of cells. Cells are harvested at

specified time points, and proliferation is quantified by counting the number of cells following trypan blue staining. An alternative is to measure the activity of succinate-tetrazolium reductase, which is active in living cells and inactive in dead cells. The second analytic method is incubating proliferating cells with thymidine analogs, such as tritiated thymidine, bromodeoxyuridine (BrdU), and ethynyldeoxyuridine. Cells that have proliferated are identified by the presence of thymidine analogs post-incubation, which are incorporated into the genome during S-phase. The third method is to detect proliferation markers by immunostaining. Cells are fixed and stained with specific antibodies that target, for instance, the cell proliferation marker Ki-67, the S-phase marker PCNA, or the M-phase marker phospho-histone H3.

Although these conventional methods are widely used, they have a number of limitations. The data obtained by these methods consist of sample values harvested from different cultures for each time point and are not a continuous observation of the same culture. These methods are unsuitable for analyzing the proliferative ability of a particular cell type or group of interest in a heterogeneous population. While staining for proliferation markers can detect proliferating cells in a specific group, these results are only snapshots of growth. Therefore, a novel method complementary to these conventional proliferation assays is sorely needed.

Extracellular signaling molecules can stimulate proliferation. Interleukin-6 (IL-6) is a secreted protein encoded by the *IL6* gene. IL-6 forms a heterocomplex with the IL-6 receptor and glycoprotein 130 on the cytoplasmic membrane, which activates the Janus kinase/signal transduction and activator of transcription 3 (STAT3)

intracellular signaling pathway [12, 13]. IL-6 secretion is high in basal-like breast cancer, a cancer subtype that possesses high proliferative and metastatic ability [14-16]. IL-6 secreted by cancer cells has been suggested to have paracrine effects in this type of breast cancer. In terms of cell proliferation, however, the involvement of IL-6 is controversial (reviewed in [17]), as administration of IL-6 has been reported to variously inhibit, enhance, or have no effect on cell proliferation [17]. Further study with novel techniques will provide a new insight into the function of IL-6 in cancer cell proliferation.

This study describes the design of an optical labeling-based proliferation assay system (the OPA system) that utilizes a photoconvertible fluorescent protein. As the fluorescence emission wavelengths of photoconvertible proteins are changed by irradiation, we can therefore label particular cells by irradiation (optical labeling) [18, 19]. In biology research, optical labeling is known as a technique that allows researchers to trace the behavior of a single cell, as well as analyze the dynamics of a group of cells, such as group migration, distribution, and growth. Different from these approaches, the OPA system uses optical labeling to quantify cell proliferation based on the reduction in photoconverted fluorescent protein molecules per cell following cytoplasmic division.

The Kaede protein is a photoconvertible fluorescent protein whose color irreversibly changes from green to red after irradiation with short wavelength light [20]. In this study, we used the Kaede protein in the OPA system. We detected reductions in the fluorescence of photoconverted Kaede by simply taking pictures and measuring its intensity in living cells, thus successfully quantifying proliferation. The OPA system

enables us to perform observations of cell proliferation in the same culture over time. Furthermore, we can analyze the proliferative ability of a specific group of cells in co-culture experiments by labeling the group of interest with Kaede. This study shows that the OPA system facilitates the understanding of the molecular mechanisms of cell proliferation. Using the OPA system, we examined the effect of IL-6 knockdown in breast cancer cell lines. We also analyzed the proliferation of IL-6-knockdown cells in co-culture experiments with IL-6-producing cells. Our results show the function of cancer-secreted IL-6 in cancer cell proliferation.

2. Materials and Methods

2.1. Cell culture

Basal-like breast cancer cell lines Hs578T and MDA-MB-231, and luminal breast cancer cell line MCF-7 were obtained from American Type Culture Collection (Manassas, VA, USA). Hs578T and MDA-MB-231 cells were maintained with Dulbecco's Modified Eagle Medium (DMEM) (Sigma, R8758, St. Louis, MO, USA) with 10% fetal bovine serum (FBS). MCF-7 cells were cultured with RPMI-1640 (Sigma, D5796) containing 10% FBS and 1 nM estradiol (Sigma, E2758). Lenti-X 293T cells (Takara Bio, 632180, Otsu, Japan), used to produce lentiviral particles, were maintained with DMEM containing 10% FBS. To obtain Kaede-expressing cell lines and shRNA-expressing cells, drug selection was performed. We used 10 μg/mL blasticidin for Kaede-expressing cells, and 1 μg/mL puromycin for shRNA-expressing cells.

To analyze proliferation using the OPA system, cells were cultured with phenol red-free media to reduce the background fluorescence: i.e., phenol red-free DMEM (Wako, 044-32955, Osaka, Japan) with 10% FBS for Hs578T and MDA-MB-231 cells, and phenol red-free RPMI-1640 (Life Technologies, 11835-030, Carlsbad, CA, USA) with 10% FBS and 1 nM estradiol for MCF-7 cells.

Mitomycin C (MMC) was used to pharmacologically inhibit proliferation. MMC was purchased from Wako (133-15931). Control groups were treated with the vehicle, i.e., 10% ethanol in ethylene glycol.

To measure the red intensity of entire well, we used a microplate reader, Spectra Max Gemini EM (Molecular Devices, Sunnyvale, CA, USA). In 1 day prior to assay, $1x10^4$ cells per well were plated in a 96-well plate. Red fluorescence was excited with 544 nm light, and detected as 590 nm light. Data were collected with Soft Max Pro 5 software (Molecular Devices). Values were normalized to the non-photoconverted control.

2.2. Vector construction

To introduce Kaede and shRNA expression, we used lentiviral vectors. For Kaede expression, we used pLenti 6.3 vector (Life Technologies, V533-06), which has a CMV promoter. The *Kaede* gene was purchased from Medical and Biological Laboratories (AM-V0011, Nagoya, Japan). We added a synthesized nuclear localization signal (NLS)-FLAG sequence to the 3' region of the *Kaede* gene in order to construct a Kaede-NLS-FLAG fusion gene. The Kaede-NLS-FLAG fusion gene was inserted

downstream of the CMV promoter of the pLenti 6.3 vector.

For shRNA-mediated gene silencing, we used a pLKO.1 vector (Addgene, 8453), which expresses the inserted shRNA sequence by human U6 promoter. The synthesized shRNA template was inserted between the *Age*I *Eco*RI sites of the pLKO.1 vector. The shGFP and shBMI1 sequences have been described previously [21]. The shIL6 sequence used was validated by a previous study [15].

2.3. Immunostaining

Immunostaining was performed to detect Kaede, pSTAT3 and STAT3 proteins, and cyclobutane pyrimidine dimers in fixed cells. The procedure has been described previously [21]. Cells were fixed with 4% paraformaldehyde for 15 min at room temperature. Permeabilization was performed with 10 μg/mL proteinase K (Wako, 169-21041) in phosphate-buffered saline (PBS) on ice for 2 min. Primary antibodies used were mouse anti-FLAG M2 antibody (Sigma, F1804, 1/300 dilution), mouse anti-cyclobutane pyrimidine dimers antibody TDM-2 (Cosmo Bio, NMDND001, Tokyo, Japan, 1/1500 dilution), rabbit anti-phospho-STAT3 Tyr705 (D3A7) (Cell Signaling technology, X9145, Danvers, MA, USA, 1/100 dilution) and rabbit anti-STAT3 antibody (D3Z2G) (Cell Signaling Technology, 12640, 1/300 dilution). To detect primary antibody binding via fluorescence microscopy, we used secondary antibodies, goat anti-mouse IgG antibody conjugated to Alexa Fluor 488 (Life Technologies, A11001, 1/1000 dilution), and goat anti-rabbit IgG antibody conjugated to Alexa Fluor 546 (Life Technologies, A11010, 1/1000 dilution). Counter staining was performed

with Hoechst 33342 (Dojindo, 346-07951, Kamimashiki, Japan, 1/1000 dilution).

2.4. TdT-mediated dUTP nick end labeling assay

To detect dead cells, we performed a TdT-mediated dUTP nick end labeling (TUNEL) assay using an *in situ* cell death kit (Roche, 11 684 817 910, Mannheim, Germany). The TUNEL signal was enhanced by goat anti-fluorescein antibody conjugated to Alexa Fluor 488 (Life Technologies, A11096, 1/500 dilution). We analyzed cells at 24 hours post-irradiation (hpi).

2.5. Imaging

To determine whether Kaede molecule localizes to the nuclei, and to perform time-lapse imaging, a confocal platform, TCS SP8 (Leica, Tokyo, Japan), was used to collect fluorescence and bright field images. Hoechst 33342 signal was excited by 405 nm light and detected with 410-470 nm light, while Alexa Fluor 488 was excited by 488 nm light and detected with 500-550 nm light. The excitation and detection wavelengths of Kaede-red were 561 nm and 570-700 nm, respectively. In time-lapse analyses, 4 optical sections were collected at 2.5-μm intervals and projected. Cell cultures were photoconverted, and then placed on the microscope stage in a humid chamber. During time-lapse analysis, the temperature and CO_2 concentration were maintained at 37 °C and 5%, respectively. Images were collected with the BrightR mode of TCS SP8 with a HyD detector, a highly sensitive detection system that has no detectable quenching effects on a specimen.

In order to observe Kaede-red fluorescence, the immunostaining signals and the TUNEL signals, images were captured by an all-in-one BZ-9000 microscope (Keyence, Osaka, Japan). The excitation wavelengths were 340-380 nm for blue fluorescence, 450-490 nm for green florescence and 525-555 nm for red fluorescence. The detection wavelengths were 435-490 nm for blue fluorescence, 510-560 nm for green florescence and 577-632 nm for red fluorescence.

2.6. Kaede photoconversion and quantification of proliferation

For analysis of proliferation using the OPA system, $5x10^4$ cells per well were plated in a 24-well plate in 1 day prior to photoconversion. We used polystyrene 24-well plate (BD Bioscience, 353047, San Diego, CA, USA) for all-in-one microscope, and glass bottom dish (Matsunami glass, D141400, Osaka, Japan) for confocal imaging. To change the Kaede fluorescence color, cultures was placed on the all-in-one microscope stage and exposed to the excitation light for blue fluorescence, which irradiated the culture from underneath through a 10x objective lens, for 15 min at room temperature. The numerical aperture of the 10x objectibve lens used is 0.45. It has aberration correction, and is UV transmissive.

To quantify the red intensity, images were captured immediately after photoconversion, and at day 1, day 2, day 3, and day 4 post-photoconversion. All pictures for quantification were taken with a 1/2.5 sec exposure for the green signal, and with a 1 sec exposure for the red signal with a 10x objective lens. In order to avoid analyzing saturated signals, we checked against the saturation indicator of the

microscope system we used. Pictures were taken at the same position in the same culture at each time point. Cell number in each picture was counted manually. Fluorescence intensity was measured using ImageJ software. We outlined each nucleus manually, and measured its mean fluorescent intensity. We randomly measured 50 cells and calculated the mean red intensity in each picture. The relative red intensity was calculated by dividing the mean value of each point by the mean value immediately after photoconversion.

2.7. Immunoblotting

To analyze p53 protein level, we performed immunoblotting with rabbit anti-p53 antibody (N-terminal) (Epitomics, 1005-1, Burlingame, CA, USA, 1/500 dilution). Rather than using secondary antibody to probe for primary antibody binding, the Easy-Western-II detection system (Beacle, BCL-EZS21, Kyoto, Japan) was employed. For an internal control, we used mouse anti-β-actin antibody (Abcam, ab6276, Cambridge, UK, 1/5000 dilution), and goat anti-mouse IgG antibody conjugated to a peroxidase (Pierce biotechnology, 31340, Rockford, IL, USA, 1/50000 dilution). The chemical luminescence reagent used was ECL Select (GE Healthcare, Buckinghamshire, UK). Signals were detected by Ez-Capture II (ATTO, Tokyo, Japan) with ImageSaver5 software (ATTO).

2.8. Quantification of mRNA level

Procedures for total RNA extraction and cDNA synthesis have been described

previously [22], as have the protocols for quantitative reverse transcription polymerase chain reaction (RT-PCR), data analysis, and primer sequences [21]. In brief, 1 μg of total RNA was reverse transcribed with SuperScript III (Life Technologies). Quantitative RT-PCR was performed with FastStart Universal SYBR Green Master (Roche, Mannheim, Germany). Amplification of *EF1A1* was used as an internal control. The relative mRNA level and standard deviation were calculated according to instructions provided by Applied Biosystems.

2.9. BrdU labeling

To label proliferated cells with BrdU, we cultured cells with 5 μM BrdU for 1 or 2 days. BrdU labeling, permeabilization and DNaseI treatment were performed using a BrdU Flow kit (BD Bioscience, 559619). BrdU detection was performed with an anti-BrdU mouse monoclonal antibody (clone MoBU-1) conjugated to Alexa Fluor 647 (Life Technologies, B35133, 1/100 dilution).

2.10. Flow cytometry

To analyze the fluorescence of a group of cells, we performed flow cytometry. The Kaede-red signal and anti-BrdU antibody signal were detected with the FL2 and FL4 channels of the FACS Aria II (BD Bioscience), respectively. Ten thousand cells were run for each sample. Acquired data were analyzed with FlowJo software (Tomy Digital Biology, Tokyo, Japan).

2.11. Enzyme-linked immunosorbent assay

To analyze the IL-6 levels in the supernatant, we performed enzyme-linked immunosorbent assay (ELISA) with a Quantikine ELISA Human IL-6 Immunoassay (R and D Systems, Minneapolis, MN, USA). In order to prepare supernatant samples, we removed the culture medium, added 300 μL of fresh medium, and incubated for 24 hours in a 24-well culture plate. The supernatant was then sampled. Cell number was counted by manually after supernatant sampling, and used to adjust the volume of supernatant sample to $1x10^5$ cells. We used 50 μL of adjusted supernatant. ELISA for IL-6 was performed according to the manufacturer's instructions.

2.12. Statistics

The relative cell numbers, relative red intensities, and results from quantitative RT-PCR and ELISA were analyzed with Student's *t*-test. Fisher's exact test was used in order to analyze the results of the TUNEL assay. $P < 0.05$ was considered statistically significant. Error bars in all graphs indicate standard deviations.

3 Results

3.1. Introducing the expression of the photoconvertible fluorescent protein Kaede into breast cancer cell lines

Newly synthesized Kaede molecules fluoresce green (supplementary Fig. S1). Irradiation with ultraviolet or short wavelength light irreversibly converts the fluorescence from green to red. The red photoconverted form of Kaede (Kaede-red) is

not generated spontaneously under normal cell culture conditions. When a cell divides, cellular components, including Kaede-red, are distributed into the two daughter cells. In this manner, the quantity of Kaede-red molecules per cell is reduced after every division (Fig. 1A). Given that the fluorescence intensity of a cell reflects the amount of the fluorescent protein present, a reduction in Kaede-red intensity indicates that a cell has divided. This allows quantification of cell proliferation by comparing the red fluorescence intensity at a particular analysis point with the intensity immediately after photoconversion (relative red intensity). This method simply requires taking pictures and measuring the red intensities. As sampling from the culture is not required, proliferation can be observed over time in the same culture dish. This method also allows analysis of the proliferative ability of a specific group of cells in a heterogeneous population by labeling the specific group with Kaede, for example, in a co-culture assay with non-labeled cells. In this study, we aimed to establish the OPA system using the photoconvertible fluorescent protein, Kaede.

To introduce Kaede expression into cell lines, we constructed a vector consisting of the CMV promoter and the *Kaede* gene with an NLS and a FLAG tag (Fig. 1B). The Kaede-NLS-FLAG molecule (hereafter referred to simply as Kaede) localizes to the nucleus. This nuclear Kaede signal enables easy identification of each cell, even under conditions of high cell density. The nuclear signal is distinct in living cells and is distinguishable from the autofluorescence of dead cells. This allows us to measure the Kaede-red intensity, focusing on living cells. We introduced the construct into three breast cancer cell lines, Hs578T, MDA-MB-231, and MCF-7 cells, and obtained stable

clones. Hs578T and MDA-MB-231 cells are classified as basal-like breast cancers, and have high proliferative ability. MCF-7 cells are luminal breast cancer cells. MCF-7 cells exhibit strong cell-to-cell adhesion under laboratory conditions, and possess lower proliferative ability than Hs578T and MDA-MB-231 cells. To confirm that the synthesized Kaede localizes to the nucleus, we used an anti-FLAG antibody to immunostain the FLAG tag of Kaede (Fig. 1C,D; supplementary Fig. S2). Confocal imaging demonstrated that the FLAG signals overlapped with the Hoechst signals, indicating that Kaede was in the nucleus. The FLAG signal was not detected in uninfected control cells.

The color of Kaede fluorescence shifts to red by irradiation with short wavelength light. In this study, we used a wavelength of 340-380 nm, a light for blue fluorescence excitation. To change the color of Kaede, a culture was set on a fluorescence microscope stage and exposed to light at 340-380 nm for 15 min at room temperature (Fig. 1E). Prior to irradiation, green fluorescence, but not red fluorescence, was observed (Fig. 1F), indicating that Kaede-red is not generated under standard cell culture conditions. Green fluorescence was reduced by exposure to 340-380 nm wavelengths, and red fluorescence became detectable (Fig. 1G). Therefore, this Kaede expression system evidently enables the labeling of cells with Kaede-red by irradiation with 340-380 nm light.

3.2. No detectable cellular damage following the Kaede photoconversion procedure

To analyze proliferation using the OPA system, photoconversion is required. While

ultraviolet irradiation is an effective way to change the color of Kaede fluorescence [20, 23], exposure of cells to strong ultraviolet light can lead to cellular damage and the initiation of a stress response [24-26], both of which can affect cell growth. Therefore, photoconversion conditions whereby no cellular damage or stress occurs are required. Accordingly, this study photoconverted Kaede by irradiation with 340-380 nm light, which is milder than irradiation from an ultraviolet lamp.

We analyzed whether our photoconversion conditions caused cellular damage. To examine the effect of photoconversion on cell growth, pictures were taken in the same position immediately after photoconversion (day 0), and up to day 4 post-irradiation. Cells were counted, and the numbers relative to the number of cells at day 0 in each culture were analyzed. Relative cell numbers of cultures exposed to 340-380 nm light did not change significantly at any time point relative to the unirradiated control (Fig. 2A,B). We next analyzed cell death via TUNEL assay. Cells were irradiated with 340–380 nm light, incubated for 24 hours, and TUNEL-positive cells was identified (Fig. 2C,D). Exposure to light from an ultraviolet lamp for 2 min was used as a positive control for cellular damage (Fig. 2E). The peak wavelength of light from the ultraviolet lamp used is 257.3 nm, which is stronger ultraviolet light than 340-380 nm. The ratio of TUNEL-positive cells did not significantly differ between cultures irradiated with 340-380 nm light and the negative control (Fig. 2F; supplementary Table S1). These results indicate that under these photoconversion conditions, cell proliferation and survival are unaffected.

At the molecular level, ultraviolet light irradiation generates dimers between

two adjacent pyrimidine residues in nucleotide strands, referred to as cyclobutane pyrimidine dimers [27]. We used an antibody specific for the cyclobutane pyrimidine dimer to detect their presence [28]. No positive staining was observed in either the negative control or the photoconverted cells (Fig. 2G,H), unlike in cells exposed to ultraviolet light (Fig. 2I). In response to cellular stress, such as irradiation with ultraviolet light, the p53 protein is stabilized and the transcription of p53-regulated genes is altered [24, 29]. We analyzed whether our photoconversion conditions causes p53 stabilization and changes the expression of *CDKN1A*, a p53-regulated gene. Due to the p53 mutation in cell lines Hs578T and MDA-MB-231, we used MCF-7 cells, which have an intact p53 gene. We detected an increase in p53 protein levels in the cells exposed to ultraviolet light at 12 hpi, compared with the negative control. As our photoconversion conditions are milder than ultraviolet irradiation, we also analyzed the cells at 6 and 12 hpi. In contrast to ultraviolet irradiation, no change in p53 level was observed under these photoconversion conditions at either 6 or 12 hpi (Fig. 2J). *CDKN1A* transcription is positively regulated by p53. We performed quantitative RT-PCR analysis for *CDKN1A*. The mean value of the control receiving no irradiation was defined as 1. No up-regulation of *CDKN1A* expression was observed in cells exposed under our photoconversion conditions, whereas a 5-fold increase in expression was seen following ultraviolet irradiation (Fig. 2K). No detectable changes in the cyclobutane pyrimidine dimer signal, the p53 protein level and the *CDKN1A* transcription level indicate that irradiation with 340-380 nm light for 15 min does not cause cellular stress at the molecular level. Therefore, these specific irradiation

conditions can be used to convert the fluorescence of Kaede without risk of cellular or molecular damage.

3.3. Reduction in Kaede-red intensity by cell division

The amount of Kaede-red per cell reduces after every cell division. To observe the reduction in red intensity, time-lapse imaging was performed beginning immediately after photoconversion (supplementary Movie). The reduction patterns of the red intensity were similar in almost all actively proliferating cells and the red intensity of the whole group changed homogeneously, indicating that the OPA system with Kaede is suitable for analyzing the proliferation of a group of cells. To examine the behavior of each cell in detail, we analyzed the movie frame-by-frame, and traced each cell. Figure 3A shows a representative cell division event. In this figure, the cell initiated division at the time point 2h:20min. Kaede-red dispersed into the cytoplasm at 3:20, suggesting that the nuclear membrane had dissolved. The cell divided at 4:00. Nuclear membranes were re-formed and Kaede-red once again localized to the nuclei at 5:00.

To quantify changes in red intensity, we measured the mean intensity of each nucleus. This measurement would not be valid, however, if the nucleus size varied among cells. Reassuringly, the size of nucleus did not markedly differ in each of the breast cancer cell lines examined, i.e., Hs578T, MDA-MB-231, and MCF-7 cells (supplementary Table S2). Therefore we used the mean intensity of each nucleus in the following analyses. Although fluorescence is quenched by time-lapse microscopy, we did not observe a reduction in fluorescence after 30 (5 h) or 60 (10 h) observations in

cells that did not divide during analysis (Fig. 3B).

If a cellular component is distributed equally between the two daughter cells, the red intensity would theoretically be halved after cell division. We measured the red intensities before a cell underwent cell division and after the re-formation of the nuclear membrane in the daughter cells. Relative values were calculated by dividing the intensity after a division by the intensity before a division. Although the value did not consistently halve every division, the mean relative values over 50 divisions (100 daughter cells) were approximately half their original intensities in Hs578T, MDA-MB-231, and MCF-7 cells (Fig. 3C; supplementary Table S3). We analyzed the distribution of Kaede-red intensity in the population of photoconverted cells by flow cytometry, and observed that the intensity was tightly distributed (supplementary Fig. S3). These results imply that the red intensity of a given cell is reduced each time that it divides, and that proliferation can be quantified by calculating the mean relative value of a group of cells.

To analyze whether the red fluorescence is retained if a cell is not proliferating, we used MMC, a chemical that inhibits cell proliferation. MMC treatment indeed inhibited cell proliferation in this study (supplementary Fig. S4A). To analyze proliferation using the OPA system, we measured the red fluorescence at day 0 and day 3, and the relative red intensity between these time points was calculated (Fig. 3D). Given that the relative values would be inaccurate if saturated images were used, we checked the images using the saturation indicator of the microscope to ensure that only unsaturated signals were analyzed. Compared with the red fluorescence at day 0, the

fluorescence was decreased at day 3 in the control cultures (Fig. 3E), but not in the MMC-treated group (Fig. 3F), indicating that low or non-proliferating cells retain high red intensity. These results affirm that the proliferative ability of cells can be evaluated using the OPA system. In cell culture, cells move actively. As the OPA system analyzes the mean relative value of a group of photoconverted cells, it can evaluate proliferation if some cells migrate out of or enter the frame.

The change in red intensity at day 3 relative to day 0 reflected change in cell number (Fig. 3D). We also analyzed the change in red intensity relative to the value of total Kaede intensity (green + red) (supplementary Fig. S4B), finding that the total Kaede intensity of the MMC-treated group decreased, even though the cell number and relative red intensity was unchanged compared with day 0 (supplementary Fig. S4A; Fig. 3D). This discrepancy appears to be due to the change in total Kaede intensity (supplementary Fig. S4C). An increase in total Kaede intensity was observed in MMC-treated cells at day 3 compared with day 0. In proliferating cells, newly synthesized green Kaede is reduced by cell division. However, in non-proliferating cells, such as MMC-treated cells, newly synthesized green Kaede accumulates, resulting in an increase in the total Kaede fluorescence of non-proliferating cells, as well as a difference in the total Kaede intensity between proliferating and non-proliferating cells. These results indicate that using red intensity relative to day 0, rather than to total Kaede intensity, is simpler and more suitable for evaluating changes in proliferation.

3.4. Quantification and time course analysis of cell proliferation using the OPA system

with Kaede

To quantify cell proliferation and to perform a time course analysis, Kaede-expressing cells were cultured and photoconverted. Pictures were taken immediately after photoconversion, and at day 1, day 2, day 3, and day 4 post-irradiation (Fig. 4A). Cells were treated with MMC or the vehicle after photoconversion to test whether the OPA system could quantify changes in proliferative ability.

In the OPA system, proliferating cells have low Kaede-red intensity. To show this, we analyzed changes in the relative cell number and the relative red intensity, which were calculated by dividing their respective value at a particular analysis point by the time point immediately after photoconversion. The relative cell number of the Hs578T cell control increased from day 1 to day 4 (Fig. 4B), with the corresponding relative red intensity of the same culture declining each day (Fig. 4C). As expected, the mean red intensity halved when the mean cell number doubled (Fig. 4B,C at day 2, control). In addition, the mean red intensity became one third of the original day 0 value when the mean cell number increased by 300% (Fig. 4B,C at day 3, control). Together, these data indicate that a reduction in the mean red intensity of the group reflects the degree of cell proliferation. On the other hand, cultures treated with 1 μg/mL MMC did not grow (Fig. 4B) and the red intensity did not remarkably decrease (Fig. 4C), indicating that inhibiting proliferation causes retention of the red fluorescence intensity. Similar patterns of increasing relative cell number and decreasing red intensity were observed in the control groups of MDA-MB-231 (Fig. 4D,E) and MCF-7 cells (Fig. 4F,G). As treatment with 1 μg/mL MMC over 4 days was toxic to MDA-MB-231 cells,

0.5 μg/mL MMC was used in these cultures instead. The mean red intensity did not decrease in MDA-MB-231 cells when cell proliferation was inhibited with MMC (Fig. 4E). In MCF-7 cells, a significant effect of MMC was observed at day 3 and day 4 (Fig. 4F,G). The red intensity did not decrease from day 3 to day 4 (day 3 vs. day 4, $P = 0.14$), during which the cell number did not increase. This result indicates that MCF-7 cells are not sensitive to 1 μg/mL of MMC compared with basal-like breast cancer cells.

In addition to pharmacological inhibition of cell proliferation, we performed genetic inhibition in MDA-MB-231 cells. We used shRNA-mediated gene silencing for the *BMI1* gene, which encodes a polycomb protein. BMI1 epigenetically suppresses cyclin-dependent kinase inhibitor genes. Therefore BMI1 knockdown leads to the expression of cyclin-dependent kinase inhibitors, resulting in the inhibition of cell proliferation. Indeed, MDA-MB-231 cells with BMI1 knockdown exhibited inhibition of cell proliferation (Fig. 4H) and no reduction in red intensity (Fig. 4I). High Kaede-red intensity was maintained in non-proliferating BMI1-knockdown cells, suggesting that Kaede-red is stable enough for use in the proliferation assays lasting 4 days. To further analyze the stability of Kaede-red, we measured the red intensity of the entire well (supplementary Fig. S5). We observed no change in red intensity over 4 days in the control or MMC-treated cells, although a slight reduction in red intensity was observed in MMC-treated Hs578T and MDA-MB-231 cells at day 4 via the OPA system. Together, these results confirm that the OPA system can allow the evaluation of differences in proliferative ability in genetic studies, as well as in pharmacological studies.

Comparison of the OPA system with a conventional method for analyzing cell proliferation (in this case, BrdU incorporation) could help to highlight the advantages of the OPA system. Kaede-expressing cells were photoconverted and treated with 5 μM BrdU. After a 1- (Fig. 5A) or 2-day (Fig. 5B) incubation, the change in red intensity was analyzed, as was the population of BrdU-positive cells. In Hs578T cultures, the number of cells increased from day 1 to day 2 (Fig. 5C), as did the number of BrdU-positive cells (Fig. 5D). In addition, the relative Kaede-red intensity decreased, also indicative of cell proliferation (Fig. 5E). A similar pattern was observed in MDA-MB-231 (Fig. 5F,G,H) and MCF-7 cells (Fig. 5I,J,K). In high proliferative cancer cells, the number of BrdU negative cells was low at day 2 (supplementary Fig. S6), indicating that almost all cells was proliferating. However BrdU negative population was observed in a low proliferative cell line at day 2 (supplementary Fig. S6), suggesting that there are slow or non-proliferating cells.

While BrdU-positivity is also indicative of cell proliferation, and an increase in the number of BrdU-positive cells implies that the number of proliferating cells increased. BrdU labeling cannot quantitatively show how many times the cells have proliferated, nor it analyzes proliferation over time because BrdU detection requires sampling cells. In the OPA system, the reduced red intensity indicates that cells have proliferated, with the mean relative red intensity of a group demonstrating the degree of proliferation. Although both BrdU labeling and the OPA system demonstrate that proliferation has occurred, only the OPA system allows analysis of the degree of proliferation over time, as shown in Fig. 4.

3.5. Attenuation of cell proliferation by IL-6 knockdown in basal-like breast cancer

IL-6 is a secreted protein that acts as a ligand to activate STAT3 [12, 13]. Activated STAT3 positively regulates cell growth. However, the role of IL-6 signaling in breast cancer proliferation, as reviewed by Dethlefsen *et al*., is still controversial [17]. Previous studies have been done using conventional methods for analyzing cell proliferation. To examine IL-6 function in this context, we analyzed cell proliferation using the OPA system following IL-6 knockdown, allowing the analysis of the proliferation of living cells over time within the same sample.

High IL-6 secretion has been observed in basal-like breast cancer cell lines [14-16]. Consistent with previous studies, we detected high IL-6 levels in the supernatant of basal-like breast cancer cell cultures, such as Hs578T and MDA-MB-231 cells, but not in luminal breast cancer cells, such as the MCF-7 cell line (Fig. 6A). To analyze the effect of IL-6 on cell proliferation, an shRNA-mediated IL-6-knockdown system was employed. IL-6 secretion by shIL6-expressing cells was less than half of the shGFP-control (Fig. 6B). Knockdown of IL-6 elicited a significant reduction in the proliferation of basal-like breast cancer cells, i.e., Hs578T (Fig. 6C,D,E) and MDA-MB-231 cells (Fig. 6F,G,H), indicating that IL-6 positively regulates cell proliferation. Although the secreted IL-6 levels differed between Hs578T and MDA-MB-231 cells (Fig. 6A), similar effects were observed after the IL-6 knockdown (Fig. 6C,F), suggesting differences in IL-6 dependency.

On the other hand, the proliferation of MCF-7 cells was unaffected by IL-6

knockdown (Fig. 6I). Further, addition of recombinant human IL-6 did not alter the proliferation of MCF-7 cells (Fig. 6J). Our results suggest that IL-6 is involved in the cell proliferation of basal-like breast cancer cells, but not luminal breast cancer cells.

3.6. The paracrine effect of IL-6 on cell proliferation in basal-like breast cancer

It is possible that cancer cell-secreted IL-6 promotes the proliferation of other cancer cells (known as a paracrine effect). To evaluate whether IL-6 exhibits a paracrine effect in basal-like breast cancer cells, we used the OPA system in co-culture experiments with Hs578T and MDA-MB-231 cells, the proliferative abilities of both of which were reduced by IL-6 knockdown (Fig. 6C,F). The OPA system enables us to analyze the proliferative ability of a specific group of cells within in a heterogeneous population (Fig. 7A). Thus, we co-cultured Kaede-expressing cells with unlabeled cells. Kaede-red was generated by photoconversion and cell proliferation was analyzed by measuring the red intensity. We introduced shGFP (control) or shIL6 into Kaede-expressing cells and unlabeled cells. Compared with the co-culture of unlabeled shGFP cells with Kaede-labeled shGFP cells (shGFP+shGFP-Kaede), the shIL6+shGFP-Kaede showed no significant difference in the proliferation of the subset of Kaede-labeled cells (Fig. 7B,C). This result indicates that IL-6 knockdown does not affect the proliferation of other adjacent cells. After co-culturing with shGFP cells, Kaede-labeled shIL6-expressing cells exhibited comparable proliferative ability to shGFP-Kaede cells. Restoration of the proliferation of Kaede-labeled cells was not observed in the shIL6+shIL6-Kaede. These observations indicate that IL-6-producing cells (i.e., the

shGFP cells here) can rescue the proliferation of shIL6-expressing cells.

To analyze whether secreted IL-6 maintains cell proliferation in basal-like breast cancer, recombinant human IL-6 was added to cultures of cells expressing shIL6. Results showed that IL-6-treatment significantly increased cell proliferation compared with PBS treatment (Fig. 7D,E). This result indicates that restoration of the proliferation of shIL6-expressing cells in the co-culture experiments is due to cancer-secreted IL-6 rather than to cell-to-cell contact.

IL-6 signaling activates STAT3 by phosphorylating at tyrosine 705. To analyze changes in STAT3 activity in shIL6-cells, we used an antibody targeting phosphorylated tyrosine 705 on STAT3 (pSTAT3) in immunocytochemistry. Strong pSTAT3 signals were detected in cells expressing shGFP (Fig. 8A), in comparison to the weak signals observed in shIL6-cells (Fig. 8B), indicating that STAT3 activation decreased in response to attenuated of IL-6 signaling. Double-staining was performed in co-culture experiments with anti-FLAG antibodies to distinguish Kaede-labeled shIL6-expressing cells from the unlabeled co-culture partners. The reduced STAT3 activation in shIL6-Kaede cells was rescued when the cells were co-cultured with the shGFP- (Fig. 8C, yellow arrowhead), but not with shIL6-cells (Fig. 8D). The amount of STAT3 seemed to remain unchanged between shGFP- and shIL6-treated cells (supplementary Fig. S7). These results suggest that cancer-secreted IL-6 induces STAT3 activation in other cells.

Taken together, the results of the co-culture experiments and recombinant IL-6 treatments indicate that IL-6 can act in a paracrine manner in basal-like breast

cancer cells, consistent with previous studies [15, 30]. IL-6-producing cancers secrete IL-6. Specifically, IL-6 secreted by IL-6-producing cancers activates STAT3 to stimulate cell proliferation in basal-like breast cancer cells, but not in luminal breast cancer.

4. Discussion

4.1. Visualization and quantification of cell proliferation

Novel techniques exploring the cellular activity, such as proliferation, contribute to the development of cell biology. In this study, we established a new proliferation assay system, the OPA system. We used a photoconvertible fluorescent protein, Kaede, and determined that measuring the reduction in Kaede-red fluorescent intensity shows the degree of proliferation in living cells. The OPA system is useful for time-course analyses, as well as for the analyses of the proliferative ability of a specific group of cells in co-culture experiments.

Currently, various methods have been established for the visualization of cell proliferation. FUCCI is a fluorescent protein-based cell cycle imaging system [31]. FUCCI allows us to monitor cell cycle progression by fluorescence. In the FUCCI system, red and green fluorescence indicate that cells are in the G1 phase and the S to M phase, respectively. Anillin is one of the contractile ring proteins, and is involved in cytoplasmic division. Localization changes of EGFP-Anillin fusions indicate progression through the M phase [32]. Rayleigh/Raman spectroscopy provides information about changes in cellular components, such as DNA and protein.

Researchers using this spectroscope have reported observations of cell cycle progression at the single-cell level [33]. These methods visualize the dynamics of cell cycle progression via time-lapse imaging, and identify proliferating cells at a specific time point by taking a picture. Differing from these techniques, in the OPA system, the degree of reduction in red fluorescence indicates whether cell proliferation has occurred during a particular experimental period. The OPA system can trace the proliferation and it is easy to compare the proliferative abilities of the control and experimental groups.

Systems similar to the OPA system have been proposed. A previous study has documented reduction in Kaede-red intensity following cell division [34]. However, the authors concluded that it was difficult for their system to analyze cell proliferation via flow cytometry. Corroborating this previous study, we also found that Kaede fluorescence data acquired using a flow cytometer were not clear, and it was difficult to identify the signatures of proliferating cells. Instead of using flow cytometry, we therefore measured the red intensity using microscope images, and then calculated the relative values and analyzed the changes in the mean relative red intensity. The Kaede protein has been used to analyze the proliferation in zebrafish fin regeneration [35], although the proliferation was not quantified. Pulse labeling with histone 2B-GFP has been used to identify low or non-proliferating cells [36]. A commercially available cell labeling dye, carboxyfluorescein succinimidyl ester (CFSE), can also be used to quantify cell proliferation. The fluorescence of CFSE is reduced after every cell division and the degree of reduction in CFSE signal reflects the level of cell proliferation. However, due to the requirements of the CFSE detection procedure, the CFSE method

is not suited for time course analyses. By using the OPA system, we succeeded in quantitatively analyzing changes in cell proliferation over time in response to pharmacological treatments and genetic manipulation (Fig. 4). The OPA system will be valuable in future studies that require observation of cell proliferation over a specific time course.

4.2. The function of IL-6 in breast cancer cell proliferation

IL-6 is one of many extracellular signaling molecules, although its impact on cell proliferation is controversial in the context of breast cancer [17]. Inhibition of cell proliferation by adding recombinant IL-6 has been reported for luminal breast cancer cells, such as in T-47D, ZR-75-1, and MCF-7 cells [37-40], and in basal-like breast cancer cells, such as MDA-MB-231 cells [40]. There are other studies comparing the effect of IL-6 on proliferation between luminal and basal-like breast cancer subtypes [41-43]. These studies have shown that luminal cancer is more sensitive to proliferative inhibition by IL-6 than basal-like breast cancer. Studies that treated luminal breast cancer cells, i.e., MDA-MB-415 [44] and MCF-7 cells [45], with IL-6 showed no effect on proliferation. MCF10A is a normal mammary epithelial cell line. The proliferation of transformed MCF10A cells is not affected by the expression of *IL6* shRNA [46].

In contrast to these studies, positive effects of IL-6 have also been reported. Growth of MCF10A cells is enhanced by the addition of supernatants from MDA-MB-231 cultures, with an increase in STAT3 phosphorylation [14]. Administration of IL-6 also enhances the proliferation of MCF-7 cells as well as the

proliferation of a HER2-positive breast cancer cell line, BT-474 [30, 47]. In the study on MCF-7 cells, no effect was observed following administration of IL-6, although proliferation was reduced by IL-6 depletion with antibody and with antisense oligonucleotides. A reduction in proliferation by IL-6 depletion is rescued by administration of recombinant IL-6 [48]. Recombinant IL-6 increases the proliferation of the basal-like breast cancer cells Hs578T that had IL-6 knocked down [15]. It is thus evident that the effect of IL-6 treatment and IL-6 inhibition tend to vary between studies. These differences might be caused by differences in culture conditions, such as the medium used, culture scale, and cell density, and in assay methods.

In this study, we observed a reduction in proliferation after IL-6 knockdown in basal-like breast cancer cells, but not in luminal breast cancer (Fig. 6), suggesting that the function of IL-6 on proliferation differs among breast cancer subtypes. Reduction in proliferative ability after IL-6 knockdown in basal-like breast cancer was not as severe as observed after the BMI1 knockdown shown in Fig. 4I. Our IL-6 knockdown system attenuated STAT3 activation (Fig. 8). This indicates that IL-6 signaling is involved in basal-like breast cancer proliferation, but is not a major factor. Similar to previous studies [15, 48], we observed that the reduced proliferative ability of IL-6-knockdown cells could be restored by co-culturing these with IL-6-producing cells, and also by recombinant IL-6 treatment (Fig. 7). Our results indicate that basal-like breast cancer secretes IL-6 to promote the proliferation of other basal-like breast cancer cells. A previous study has shown that high STAT3 activation is observed in cancer stem cell populations, defined as $CD44^+$ $CD24^-$ cells [15]. Further study is required to understand

the function of cancer cell-secreted IL-6 in stemness, and the OPA system may facilitate the study of the role and function of IL-6 in cancer stem cell proliferation.

5. Conclusions

In this study, we visualized and quantified cell proliferation using the OPA system. We showed that IL-6 signaling positively regulates cell proliferation in basal-like breast cancer. Furthermore, we obtained direct evidence of IL-6 exhibiting a paracrine effect. Our results indicate that cancer cells can promote the proliferation of other cancer cells by secreting signaling molecules.

Conflict of interest statement

Junji Itou is an employee of Kyoto University's Sponsored Research Program funded by Taiho Pharmaceutical Co., Ltd. Sunao Tanaka, Fumiaki Sato, Ryutaro Akiyama and Yasuhiko Kawakami declare no competing interests. Masakazu Toi received research funding from Taiho Pharmaceutical Co., Ltd. The funding sources had no role in the study design, experiment, analysis, interpretation or writing the manuscript. The corresponding author had full access to the data and final responsibility for submission.

Acknowledgements

We thank Dr Kunio Kitada, Dr Yasuko Miyake, Dr Elham Fakhrejahani, Dr Fengling Pu and Ms Kayoko Koishihara for technical assistance. We thank Dr Isao Oishi and Dr Yoshiaki Matsumoto for editorial assistance. We thank the members of departments of

breast surgery, and of hepato-biliary-pancreatic surgery and transplantation for sharing laboratory equipment. Confocal imaging and time-lapse analysis using Leica TCS SP8 were performed at the Medical Research Support Center, Graduate School of Medicine, Kyoto University. This study was supported by JSPS Grant-in-Aid for Young Scientists (B) No.25870384. Financial support was provided by Taiho Pharmaceutical Cd. Ltd.

References

[1] D. Hanahan, R.A. Weinberg, Hallmarks of cancer: the next generation, Cell, 144 (2011) 646-674.

[2] M.L. Whitfield, L.K. George, G.D. Grant, C.M. Perou, Common markers of proliferation, Nature reviews. Cancer, 6 (2006) 99-106.

[3] A.A. Adjei, M. Hidalgo, Intracellular signal transduction pathway proteins as targets for cancer therapy, Journal of clinical oncology : official journal of the American Society of Clinical Oncology, 23 (2005) 5386-5403.

[4] B. Vogelstein, K.W. Kinzler, Cancer genes and the pathways they control, Nature medicine, 10 (2004) 789-799.

[5] T. Santarius, J. Shipley, D. Brewer, M.R. Stratton, C.S. Cooper, A census of amplified and overexpressed human cancer genes, Nature reviews. Cancer, 10 (2010) 59-64.

[6] W. Timp, A.P. Feinberg, Cancer as a dysregulated epigenome allowing cellular growth advantage at the expense of the host, Nature reviews. Cancer, 13 (2013) 497-510.

[7] P. Eroles, A. Bosch, J.A. Pérez-Fidalgo, A. Lluch, Molecular biology in breast cancer: intrinsic subtypes and signaling pathways, Cancer treatment reviews, 38 (2012) 698-707.

[8] M. Niepel, M. Hafner, E.A. Pace, M. Chung, D.H. Chai, L. Zhou, J.L. Muhlich, B. Schoeberl, P.K. Sorger, Analysis of growth factor signaling in genetically diverse breast cancer lines, BMC biology, 12 (2014) 20.

[9] C.M. Perou, T. Sørlie, M.B. Eisen, M. van de Rijn, S.S. Jeffrey, C.A. Rees, J.R.

Pollack, D.T. Ross, H. Johnsen, L.A. Akslen, O. Fluge, A. Pergamenschikov, C. Williams, S.X. Zhu, P.E. Lønning, A.L. Børresen-Dale, P.O. Brown, D. Botstein, Molecular portraits of human breast tumours, Nature, 406 (2000) 747-752.
[10] J.S. Parker, M. Mullins, M.C. Cheang, S. Leung, D. Voduc, T. Vickery, S. Davies, C. Fauron, X. He, Z. Hu, J.F. Quackenbush, I.J. Stijleman, J. Palazzo, J.S. Marron, A.B. Nobel, E. Mardis, T.O. Nielsen, M.J. Ellis, C.M. Perou, P.S. Bernard, Supervised risk predictor of breast cancer based on intrinsic subtypes, Journal of clinical oncology : official journal of the American Society of Clinical Oncology, 27 (2009) 1160-1167.
[11] J. Kao, K. Salari, M. Bocanegra, Y.L. Choi, L. Girard, J. Gandhi, K.A. Kwei, T. Hernandez-Boussard, P. Wang, A.F. Gazdar, J.D. Minna, J.R. Pollack, Molecular profiling of breast cancer cell lines defines relevant tumor models and provides a resource for cancer gene discovery, PloS one, 4 (2009) e6146.
[12] Y. Guo, F. Xu, T. Lu, Z. Duan, Z. Zhang, Interleukin-6 signaling pathway in targeted therapy for cancer, Cancer treatment reviews, 38 (2012) 904-910.
[13] H. Kojima, T. Inoue, H. Kunimoto, K. Nakajima, IL-6-STAT3 signaling and premature senescence, Jak-stat, 2 (2013) e25763.
[14] J.C. Lieblein, S. Ball, B. Hutzen, A.K. Sasser, H.J. Lin, T.H. Huang, B.M. Hall, J. Lin, STAT3 can be activated through paracrine signaling in breast epithelial cells, BMC cancer, 8 (2008) 302.
[15] L.L.C. Marotta, V. Almendro, A. Marusyk, M. Shipitsin, J. Schemme, S.R. Walker, N. Bloushtain-Qimron, J.J. Kim, S.A. Choudhury, R. Maruyama, Z. Wu, M. Gönen, L.A. Mulvey, M.O. Bessarabova, S.J. Huh, S.J. Silver, S.Y. Kim, S.Y. Park, H.E. Lee, K.S. Anderson, A.L. Richardson, T. Nikolskaya, Y. Nikolsky, X.S. Liu, D.E. Root, W.C. Hahn, D.A. Frank, K. Polyak, The JAK2/STAT3 signaling pathway is required for growth of CD44(+)CD24(-) stem cell-like breast cancer cells in human tumors, The Journal of clinical investigation, 121 (2011) 2723-2735.
[16] P. Sansone, G. Storci, S. Tavolari, T. Guarnieri, C. Giovannini, M. Taffurelli, C. Ceccarelli, D. Santini, P. Paterini, K.B. Marcu, P. Chieco, M. Bonafè, IL-6 triggers malignant features in mammospheres from human ductal breast carcinoma and normal mammary gland, The Journal of clinical investigation, 117 (2007) 3988-4002.
[17] C. Dethlefsen, G. Højfeldt, P. Hojman, The role of intratumoral and systemic IL-6 in breast cancer, Breast cancer research and treatment, 138 (2013) 657-664.
[18] A. Miyawaki, Fluorescent proteins in a new light, Nature biotechnology, 22 (2004)

1374-1376.
[19] S.A. McKinney, C.S. Murphy, K.L. Hazelwood, M.W. Davidson, L.L. Looger, A bright and photostable photoconvertible fluorescent protein, Nature methods, 6 (2009) 131-133.
[20] R. Ando, H. Hama, M. Yamamoto-Hino, H. Mizuno, A. Miyawaki, An optical marker based on the UV-induced green-to-red photoconversion of a fluorescent protein, Proceedings of the National Academy of Sciences of the United States of America, 99 (2002) 12651-12656.
[21] J. Itou, Y. Matsumoto, K. Yoshikawa, M. Toi, Sal-like 4 (SALL4) suppresses CDH1 expression and maintains cell dispersion in basal-like breast cancer, FEBS letters, 587 (2013) 3115-3121.
[22] J. Itou, H. Kawakami, T. Quach, M. Osterwalder, S.M. Evans, R. Zeller, Y. Kawakami, Islet1 regulates establishment of the posterior hindlimb field upstream of the Hand2-Shh morphoregulatory gene network in mouse embryos, Development (Cambridge, England), 139 (2012) 1620-1629.
[23] J. Itou, I. Oishi, H. Kawakami, T.J. Glass, J. Richter, A. Johnson, T.C. Lund, Y. Kawakami, Migration of cardiomyocytes is essential for heart regeneration in zebrafish, Development (Cambridge, England), 139 (2012) 4133-4142.
[24] W. Maltzman, L. Czyzyk, UV irradiation stimulates levels of p53 cellular tumor antigen in nontransformed mouse cells, Molecular and cellular biology, 4 (1984) 1689-1694.
[25] F. Trautinger, I. Kindås-Mügge, R.M. Knobler, H. Hönigsmann, Stress proteins in the cellular response to ultraviolet radiation, Journal of photochemistry and photobiology. B, Biology, 35 (1996) 141-148.
[26] L. Latonen, M. Laiho, Cellular UV damage responses--functions of tumor suppressor p53, Biochimica et biophysica acta, 1755 (2005) 71-89.
[27] S. Faraji, A. Dreuw, Physicochemical mechanism of light-driven DNA repair by (6-4) photolyases, Annual review of physical chemistry, 65 (2014) 275-292.
[28] T. Mori, M. Nakane, T. Hattori, T. Matsunaga, M. Ihara, O. Nikaido, Simultaneous establishment of monoclonal antibodies specific for either cyclobutane pyrimidine dimer or (6-4)photoproduct from the same mouse immunized with ultraviolet-irradiated DNA, Photochemistry and photobiology, 54 (1991) 225-232.
[29] T. Haapajärvi, L. Kivinen, A. Heiskanen, C. des Bordes, M.B. Datto, X.F. Wang,

M. Laiho, UV radiation is a transcriptional inducer of p21(Cip1/Waf1) cyclin-kinase inhibitor in a p53-independent manner, Experimental cell research, 248 (1999) 272-279.
[30] A.W. Studebaker, G. Storci, J.L. Werbeck, P. Sansone, A.K. Sasser, S. Tavolari, T. Huang, M.W. Chan, F.C. Marini, T.J. Rosol, M. Bonafé, B.M. Hall, Fibroblasts isolated from common sites of breast cancer metastasis enhance cancer cell growth rates and invasiveness in an interleukin-6-dependent manner, Cancer research, 68 (2008) 9087-9095.
[31] A. Sakaue-Sawano, H. Kurokawa, T. Morimura, A. Hanyu, H. Hama, H. Osawa, S. Kashiwagi, K. Fukami, T. Miyata, H. Miyoshi, T. Imamura, M. Ogawa, H. Masai, A. Miyawaki, Visualizing spatiotemporal dynamics of multicellular cell-cycle progression, Cell, 132 (2008) 487-498.
[32] M. Hesse, A. Raulf, G.A. Pilz, C. Haberlandt, A.M. Klein, R. Jabs, H. Zaehres, C.J. Fügemann, K. Zimmermann, J. Trebicka, A. Welz, A. Pfeifer, W. Röll, M.I. Kotlikoff, C. Steinhäuser, M. Götz, H.R. Schöler, B.K. Fleischmann, Direct visualization of cell division using high-resolution imaging of M-phase of the cell cycle, Nature communications, 3 (2012) 1076.
[33] B. Kang, L.A. Austin, M.A. El-Sayed, Real-time molecular imaging throughout the entire cell cycle by targeted plasmonic-enhanced Rayleigh/Raman spectroscopy, Nano letters, 12 (2012) 5369-5375.
[34] M. Tomura, N. Yoshida, J. Tanaka, S. Karasawa, Y. Miwa, A. Miyawaki, O. Kanagawa, Monitoring cellular movement in vivo with photoconvertible fluorescence protein "Kaede" transgenic mice, Proceedings of the National Academy of Sciences of the United States of America, 105 (2008) 10871-10876.
[35] H.Y. Moon, O.H. Kim, H.T. Kim, J.H. Choi, S.Y. Yeo, N.S. Kim, D.S. Park, H.W. Oh, K.H. You, M. De Zoysa, C.H. Kim, Establishment of a transgenic zebrafish EF1alpha:Kaede for monitoring cell proliferation during regeneration, Fish & shellfish immunology, 34 (2013) 1390-1394.
[36] R. Sottocornola, C. Lo Celso, Dormancy in the stem cell niche, Stem cell research & therapy, 3 (2012) 10.
[37] I. Tamm, I. Cardinale, J. Krueger, J.S. Murphy, L.T. May, P.B. Sehgal, Interleukin 6 decreases cell-cell association and increases motility of ductal breast carcinoma cells, The Journal of experimental medicine, 170 (1989) 1649-1669.
[38] D.N. Danforth, Jr., M.K. Sgagias, Interleukin-1 alpha and interleukin-6 act

additively to inhibit growth of MCF-7 breast cancer cells in vitro, Cancer research, 53 (1993) 1538-1545.
[39] A. Badache, N.E. Hynes, Interleukin 6 inhibits proliferation and, in cooperation with an epidermal growth factor receptor autocrine loop, increases migration of T47D breast cancer cells, Cancer research, 61 (2001) 383-391.
[40] N. Underhill-Day, J.K. Heath, Oncostatin M (OSM) cytostasis of breast tumor cells: characterization of an OSM receptor beta-specific kernel, Cancer research, 66 (2006) 10891-10901.
[41] J.J. Chiu, M.K. Sgagias, K.H. Cowan, Interleukin 6 acts as a paracrine growth factor in human mammary carcinoma cell lines, Clinical cancer research : an official journal of the American Association for Cancer Research, 2 (1996) 215-221.
[42] A.M. Douglas, G.A. Goss, R.L. Sutherland, D.J. Hilton, M.C. Berndt, N.A. Nicola, C.G. Begley, Expression and function of members of the cytokine receptor superfamily on breast cancer cells, Oncogene, 14 (1997) 661-669.
[43] K.S. Ásgeirsson, K. Ólafsdóttir, J.G. Jónasson, H.M. Ögmundsdóttir, The effects of IL-6 on cell adhesion and e-cadherin expression in breast cancer, Cytokine, 10 (1998) 720-728.
[44] Y. Morinaga, H. Suzuki, F. Takatsuki, Y. Akiyama, T. Taniyama, K. Matsushima, K. Onozaki, Contribution of IL-6 to the antiproliferative effect of IL-1 and tumor necrosis factor on tumor cell lines, Journal of immunology (Baltimore, Md. : 1950), 143 (1989) 3538-3542.
[45] P.G. Johnston, C.M. Rondinone, D. Voeller, C.J. Allegra, Identification of a protein factor secreted by 3T3-L1 preadipocytes inhibitory for the human MCF-7 breast cancer cell line, Cancer research, 52 (1992) 6860-6865.
[46] K. Leslie, S.P. Gao, M. Berishaj, K. Podsypanina, H. Ho, L. Ivashkiv, J. Bromberg, Differential interleukin-6/Stat3 signaling as a function of cellular context mediates Ras-induced transformation, Breast cancer research : BCR, 12 (2010) R80.
[47] A.K. Sasser, N.J. Sullivan, A.W. Studebaker, L.F. Hendey, A.E. Axel, B.M. Hall, Interleukin-6 is a potent growth factor for ER-alpha-positive human breast cancer, FASEB journal : official publication of the Federation of American Societies for Experimental Biology, 21 (2007) 3763-3770.
[48] X.P. Jiang, D.C. Yang, R.L. Elliott, J.F. Head, Down-regulation of expression of interleukin-6 and its receptor results in growth inhibition of MCF-7 breast cancer cells,

Anticancer research, 31 (2011) 2899-2906.

Figure Legends

Fig. 1. Design of the optical labeling-based proliferation assay system (OPA system). (A) Schematic of the OPA system with Kaede. Irradiation of Kaede-expressing cells with 340-380 nm light generates Kaede-red molecules (magenta dots). When cells expressing Kaede-red divide, Kaede-red molecules are distributed between the daughter cells, leading to a decrease in the red intensity of each cell. In the OPA system, cells with high proliferative ability have weak red intensity, while low or non-proliferative cells have stronger fluorescence. (B) The Kaede expression construct. Expression of Kaede-NLS-FLAG is under the control of the CMV promoter. (C,D) Representative confocal images of immunostaining for Kaede in Hs578T cells using an anti-FLAG antibody. The unlabeled control (C) and Kaede-labeled cells (D) are shown (n = 3 rounds of staining). C' and D' show Hoechst 33342 nuclear staining, while C'' and D'' show the merged images. (E) Photoconversion of Kaede. A culture of cells is placed on the microscope stage, and cells are irradiated with 340-380 nm light for 15 min at room temperature. (F,G) Kaede fluorescence detected by the green (F,G) and red (F',G') filter sets. Red fluorescence is not observed prior to irradiation (F'). After photoconversion, green fluorescence decreased (G), and red fluorescence appeared (G'). Bars indicate 100 μm.

Fig. 2. No detectable cellular or molecular damages and no stress response following photoconversion. (A,B) The proliferation of Hs578T (A, *n* = 4) and MBA-MB-231 cells (B, *n* = 4) after irradiation with 340-380 nm light and unirradiated control cells were analyzed. Pictures of the cultures were taken daily at the same position. The number of cells was counted, and the relative value was calculated based on an adjusted cell number at day 0 set at 100. No statistically significant changes were observed between the unirradiated control cells and cells that were irradiated with 340-380 nm light at any time points examined. (C,D,E,F) Cell death was analyzed using a TUNEL assay. Representative images of unirradiated Hs578T cells (C, *n* = 3), cells irradiated with 340-380 nm light (D, *n* = 3), and cells exposed to ultraviolet irradiation (E, *n* = 5) are shown. Hoechst 33342 was used as a counterstain (C',D',E'). The percentage of TUNEL-positive cells was calculated by dividing the number of TUNEL-positive cells by the number of cells stained by Hoechst (F, supplementary Table S1). (G,H,I) DNA damage in irradiated Hs578T cells was evaluated by immunostaining for cyclobutane pyrimidine dimers (*n* = 3). No detectable signal was observed in the negative control (G) or following irradiation with 340-380 nm light (H). DNA damage was only observed after ultraviolet irradiation (I). Hoechst 33342 staining was used to identify the nucleus (G',H',I'). (J) Immunoblotting demonstrates that increases in p53 levels were detected only in samples irradiated with ultraviolet light (*n* = 3). Anti-β-actin antibody was used as an internal control. (K) The relative mRNA level of *CDKN1A* was analyzed (*n* = 3). In comparison with the unirradiated control, *CDKN1A* expression increased significantly in ultraviolet-irradiated cells. Student's

t-test was used in A, B, and K. Fisher's exact test was used in F. n.s.: non-significant change, **: $P < 0.01$. Error bars represent the standard deviation. Bars indicate 100 μm.

Fig. 3. Reduction in Kaede-red intensity by cell division. (A) A representative series of images of dividing MDA-MB-231 cells with Kaede-red fluorescence is shown. Arrowheads indicate the same cell. White and yellow arrowheads indicate the parent and daughter cells, respectively. (B) No significant change in red intensity was observed in non-dividing cells ($n = 30$). (C) Change in Kaede-red intensity was quantified by analyzing the relative values calculated by dividing the intensity of Kaede-red after cell division by the intensity of Kaede-red before cell division ($n = 50$ divisions, supplementary Table S3). (D,E,F) Relative red intensities are shown (D). Images show the Kaede-red signal in the control MDA-MB-231 cells (E) and in MDA-MB-231 cells treated with 0.5 μg/mL MMC (F). Student's *t*-test was used to analyze significance. MMC: mitomycin C. Error bars represent the standard deviation. n.s.: non-significant change, **: $P < 0.01$. Bars indicate 50 μm in A and 100 μm in E and F.

Fig. 4. Quantification of the effects of pharmacological and genetic inhibitions of proliferation via the OPA system. (A) Pictures were taken after cultures were irradiated to generate Kaede-red at day 0. To observe the change in proliferation daily, images were taken at the same position at day 1, 2, 3, and 4 after irradiation. (B,C,D,E,F,G) Proliferation of Hs578T (B,C, 1 μg/mL MMC, $n = 4$), MDA-MB-231 (D,E, 0.5 μg/mL MMC, $n = 4$), and MCF-7 (F,G, 1 μg/mL MMC, $n = 4$) cells. The

relative cell number (B,D,F) and the relative red intensity (C,E,G) are shown. (H,I) Proliferation of MDA-MB-231 cells following BMI1 knockdown is shown (n = 4), as indicated by the relative cell number (H) and the relative red intensity (I). Student's t-test was used to analyze the significance between the experimental and control groups at each time point. n.s.: non-significant change, *: $P < 0.05$, **: $P < 0.01$. MMC: mitomycin C. Error bars represent the standard deviation.

Fig. 5. Comparison of the OPA system with BrdU labeling. (A,B) BrdU labeling and the OPA system were performed for the same culture. Cells were incubated for 1 (A) or 2 days (B). (C,D,E,F,G,H,I,J,K) Cell number relative to day 0 (C,F,I), the population of BrdU-positive cells (D,G,J), and red intensity relative to day 0 (E,H,K) in Hs578T (C,D,E, n = 4), MDA-MB-231 (D,G,J, n = 4), and MCF-7 cells (E,H,K, n = 4) are shown. Error bars represent the standard deviation.

Fig. 6. Inhibition of proliferation by IL-6 knockdown in basal-like breast cancer but not in luminal breast cancer. (A) Endogenous IL-6 secretion by Hs578T, MDA-MB-231, and MCF-7 cells, as measured by ELISA (n = 3). (B) IL-6 knockdown reduced the level of IL-6 secreted by Hs578T cells (n = 3). shGFP was used as a control. (C,D,E) The effect of shIL6 in Hs578T cells. (F,G,H) The effect of shIL6 in MDA-MB-231 cells. (C,F) Graphs show the relative red intensity in shIL6-expressing cells (n = 4). Representative pictures of the shGFP control (D,G) and shIL6-expressing cells (E,H) are shown. (I) Graph shows the effect of shIL6 in MCF-7 cells (n = 4). (J)

Administration of IL-6 had no effect on the proliferation of MCF-7 cells (n = 4). Student's t-test was used to analyze significant differences between the experimental and control groups at each time point. n.s.: non-significant change, *: $P < 0.05$, **: $P < 0.01$. Error bars represent the standard deviation. Bars indicate 100 μm.

Fig. 7. Positive regulation of cell proliferation by secreted IL-6 in basal-like breast cancer cells. (A) To analyze proliferation in co-culture experiments, Kaede-expressing cells were mixed with non-labeled cells. The culture was then photoconverted, and the proliferation of Kaede-labeled cells was analyzed by measuring the red intensity. Images are representative of the co-culture experiments (Hs578T cells). (B,C) The relative red intensities of shGFP- and shIL6-expressing Hs578T (B, n = 4) and MDA-MB-231 cells (C, n = 4) are shown. Cells were co-cultured with unlabeled shGFP- or shIL6-expressing cells. (D,E) Graphs show the effect of IL-6 administration on shIL6-expressing Hs578T cells (D, n = 4) and MDA-MB-231 cells (E, n = 4). Student's t-test was used to analyze significant differences between the experimental and control groups at each time point. n.s.: non-significant change, *: $P < 0.05$, **: $P < 0.01$. Error bars represent the standard deviation.

Fig. 8. Rescue of STAT3 activation by co-culturing with IL-6-producing cells. (A,B) Immunostaining for pSTAT3 in shGFP (A) and shIL6 cells (B) is shown. (C,D) STAT3 activation attenuated by shIL6 was restored following co-culturing with shGFP-expressing cells (C), but not with shIL6-expressing cells (D). The Kaede signal

was detected by an anti-FLAG antibody. Yellow arrowheads in C indicate pSTAT3-positive, shIL6-expressing, Kaede-labeled cells. Bars indicate 100 μm.

Itou Fig. 1

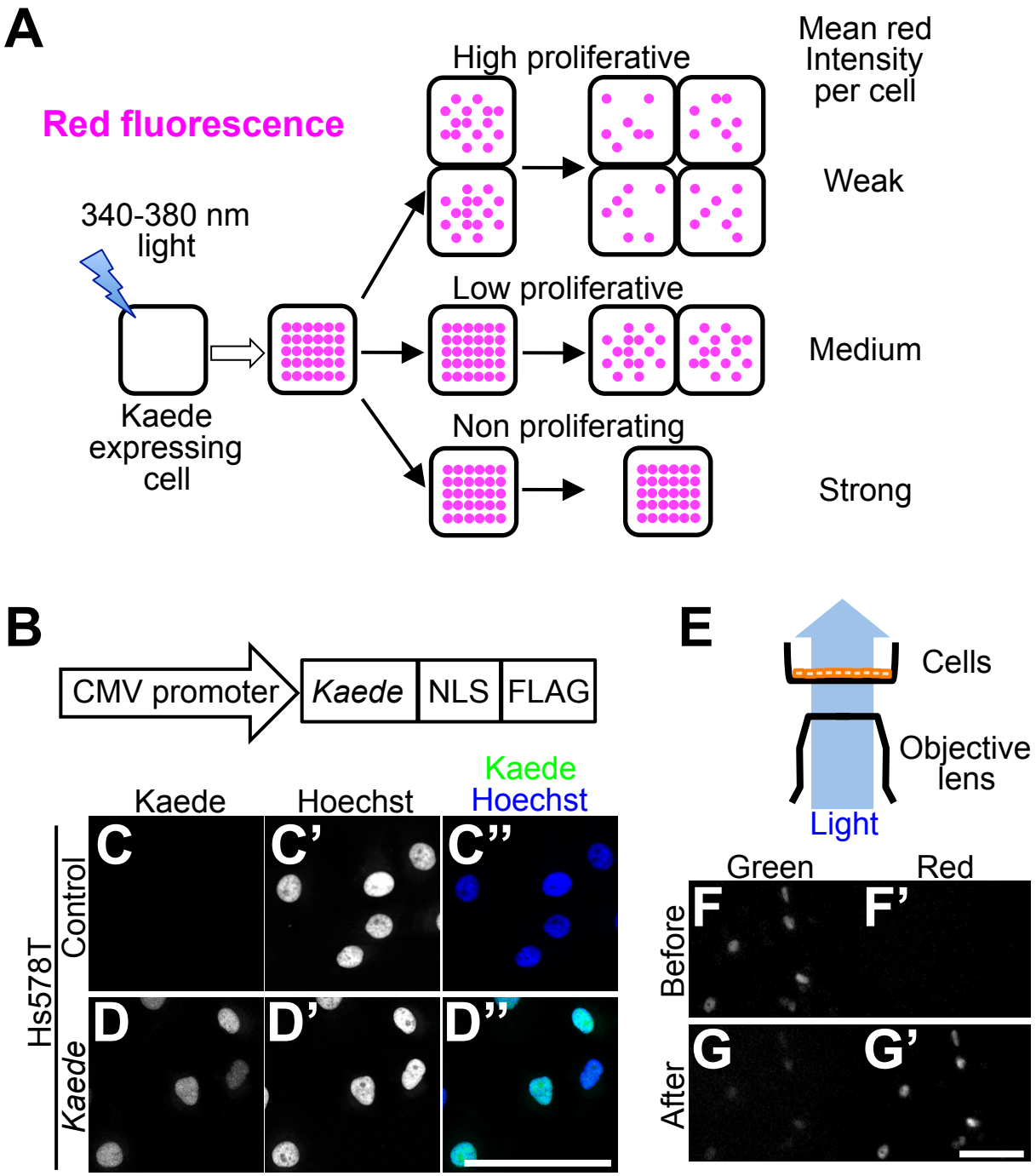
A
Red fluorescence
340-380 nm light
Kaede expressing cell
High proliferative
Low proliferative
Non proliferating
Mean red Intensity per cell
Weak
Medium
Strong
B
CMV promoter
Kaede
NLS
FLAG
Kaede
Hoechst
Kaede Hoechst
Hs578T
Control
Kaede
C
C'
C''
D
D'
D''
E
Cells
Objective lens
Light
Green
Red
Before
After
F
F'
G
G'

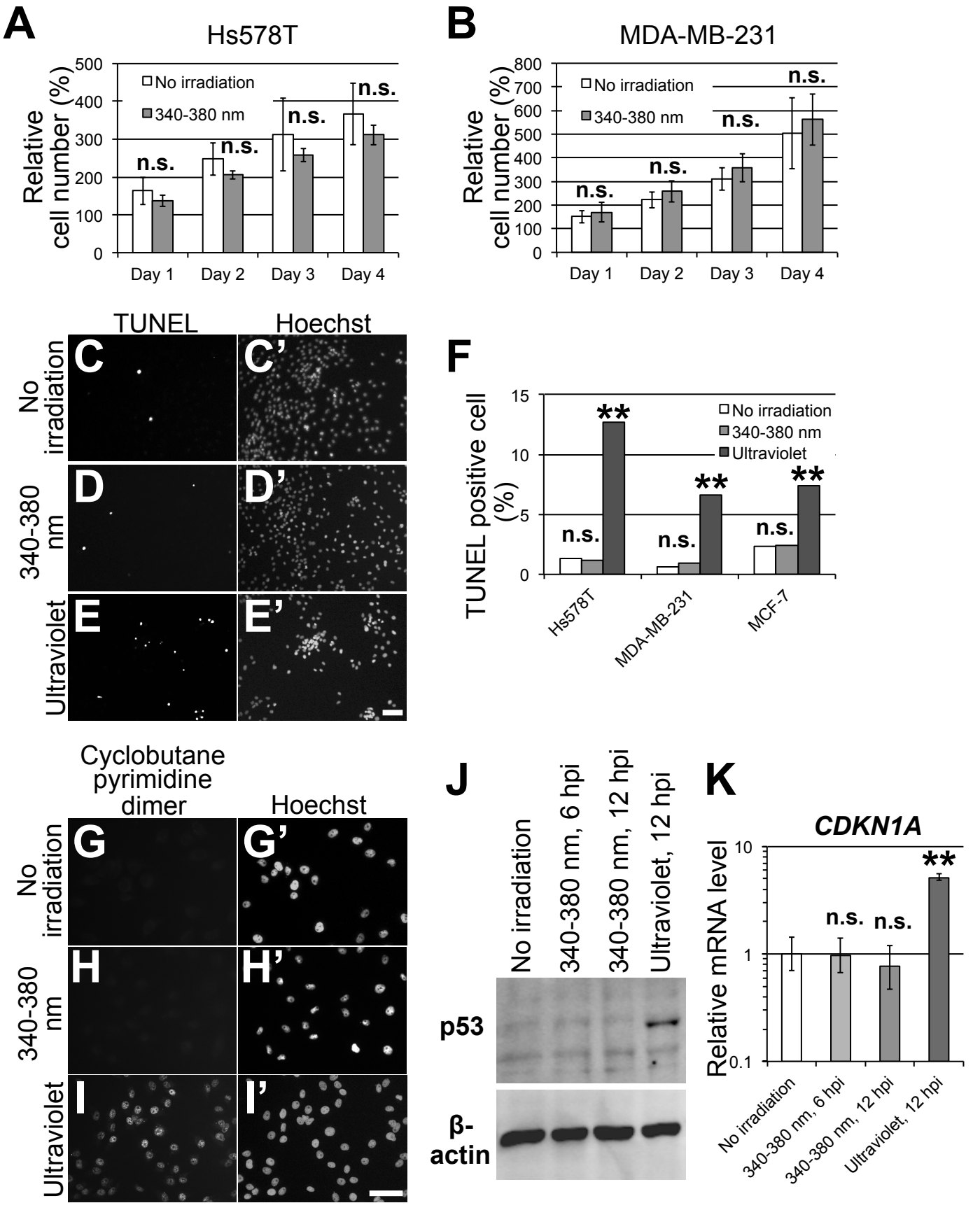
A
Hs578T
Relative cell number (%)
No irradiation
340-380 nm
n.s.
Day 1
Day 2
Day 3
Day 4
B
MDA-MB-231
TUNEL
Hoechst
C
C'
D
D'
E
E'
No irradiation
340-380 nm
Ultraviolet
F
TUNEL positive cell (%)
Ultraviolet
**
Hs578T
MDA-MB-231
MCF-7
Cyclobutane pyrimidine dimer
G
G'
H
H'
I
I'
J
No irradiation
340-380 nm, 6 hpi
340-380 nm, 12 hpi
Ultraviolet, 12 hpi
p53
β-actin
K
CDKN1A
Relative mRNA level

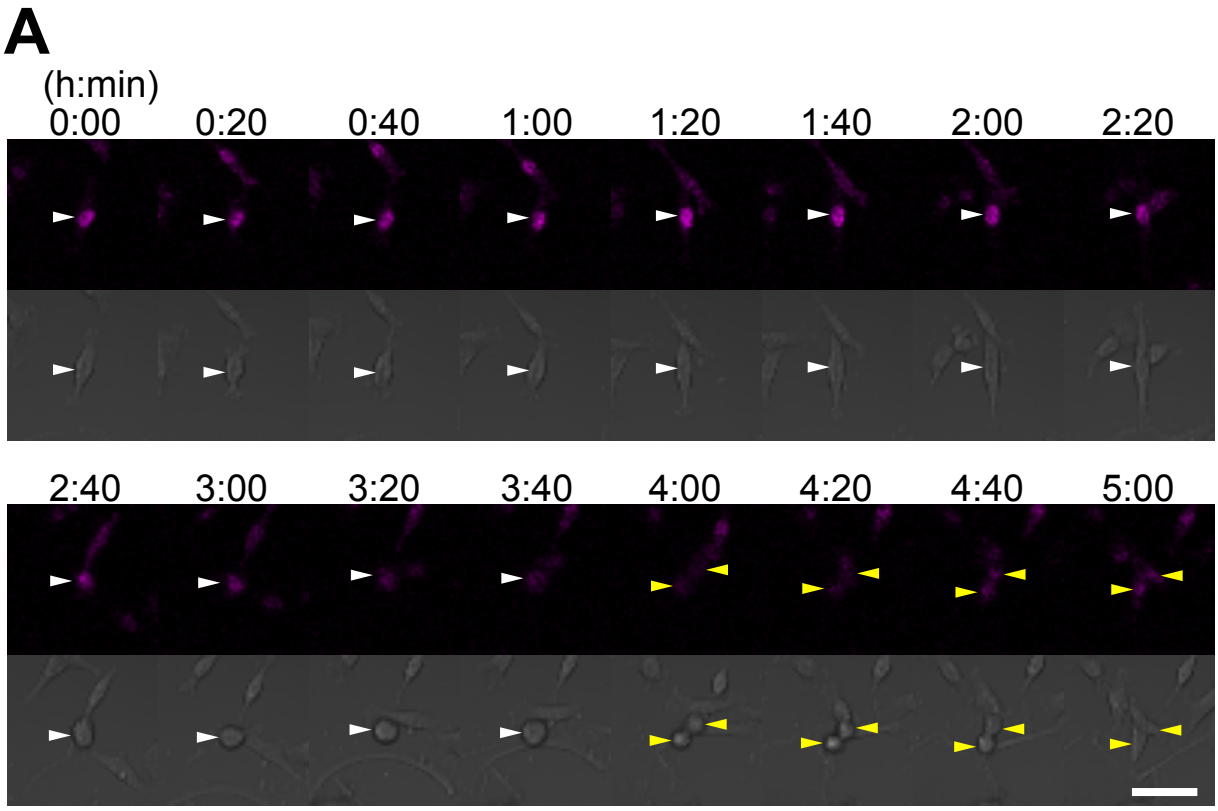
A
(h:min)
0:00
0:20
0:40
1:00
1:20
1:40
2:00
2:20
2:40
3:00
3:20
3:40
4:00
4:20
4:40
5:00

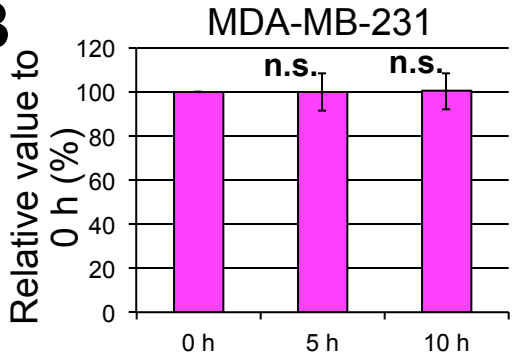
B
MDA-MB-231
Relative value to 0 h (%)
120
100
80
60
40
20
0
n.s.
n.s.
0 h
5 h
10 h

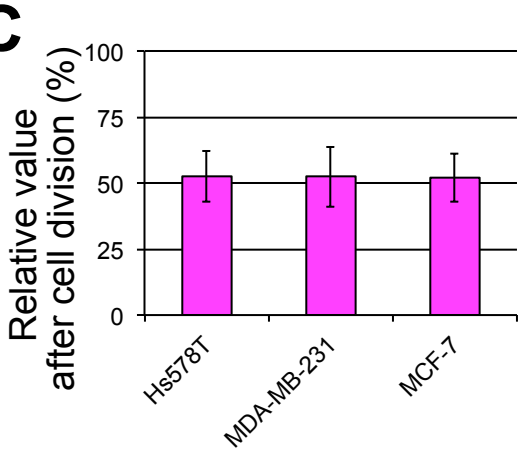
C
Relative value after cell division (%)
100
75
50
25
0
Hs578T
MDA-MB-231
MCF-7

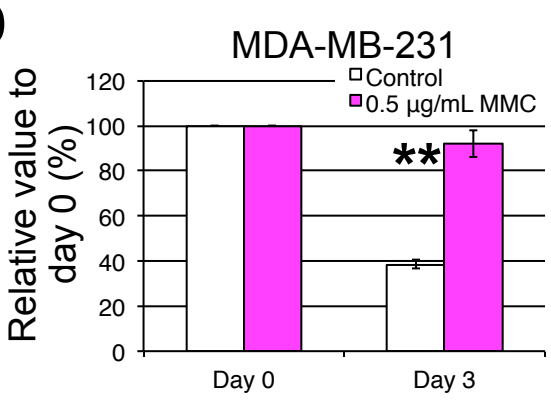
D
MDA-MB-231
Relative value to day 0 (%)
Control
0.5 µg/mL MMC
120
100
80
60
40
20
0
**
Day 0
Day 3

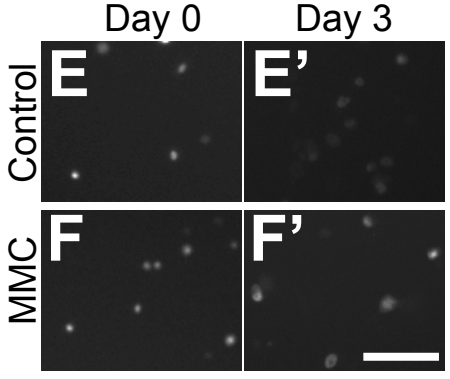
Day 0
Day 3
Control
MMC
E
E'
F
F'

Itou
Fig. 4

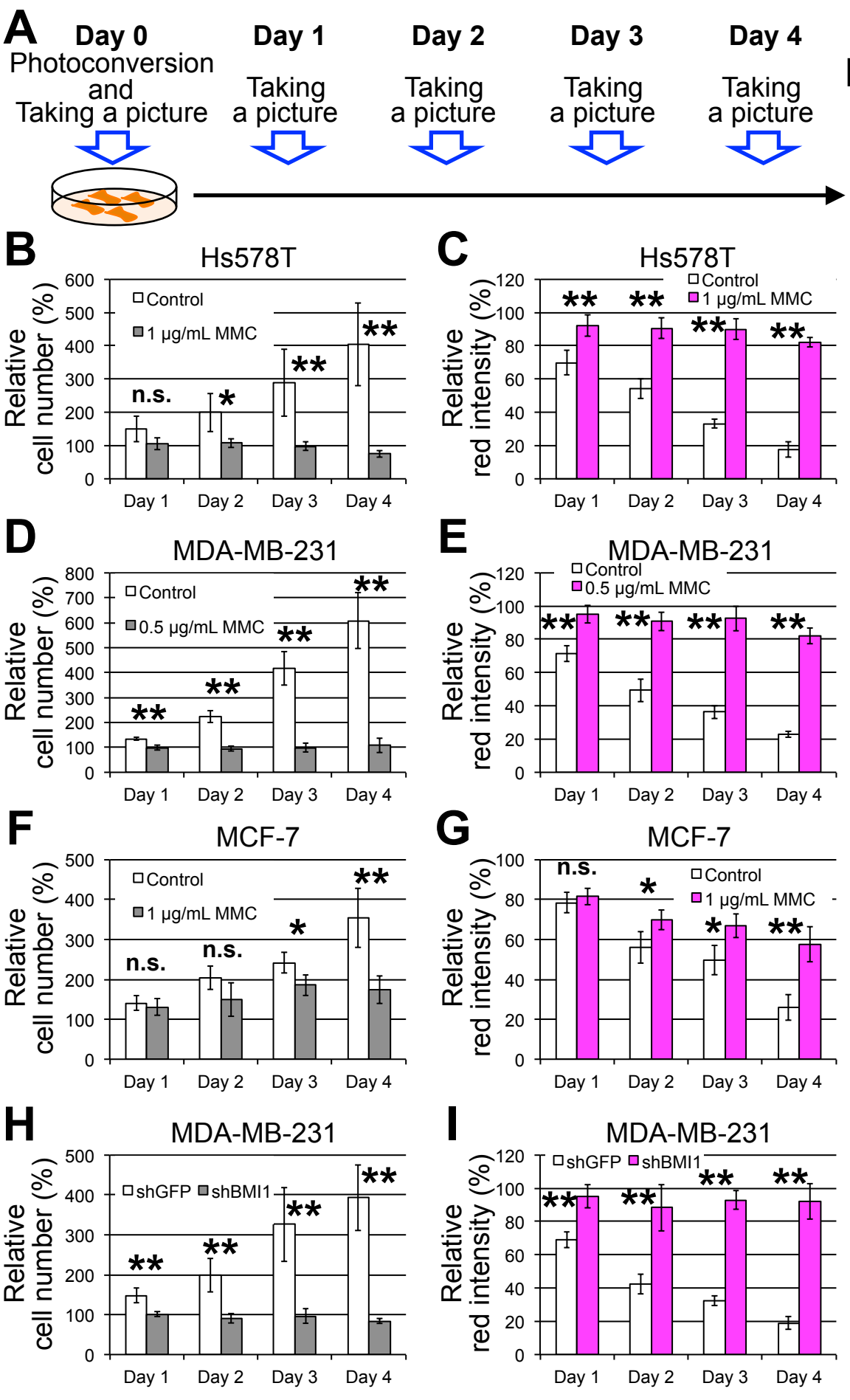
A
Day 0
Photoconversion
and
Taking a picture
Day 1
Taking
a picture
Day 2
Taking
a picture
Day 3
Taking
a picture
Day 4
Taking
a picture
B
Hs578T
Relative
cell number (%)
Control
1 μg/mL MMC
n.s.
*
**
**
Day 1
Day 2
Day 3
Day 4
C
Hs578T
Relative
red intensity (%)
Control
1 μg/mL MMC
**
**
**
**
D
MDA-MB-231
Relative
cell number (%)
Control
0.5 μg/mL MMC
**
**
**
**
E
MDA-MB-231
Relative
red intensity (%)
Control
0.5 μg/mL MMC
**
**
**
**
F
MCF-7
Relative
cell number (%)
Control
1 μg/mL MMC
n.s.
n.s.
*
**
G
MCF-7
Relative
red intensity (%)
Control
1 μg/mL MMC
n.s.
*
*
**
H
MDA-MB-231
Relative
cell number (%)
shGFP
shBMI1
**
**
**
**
I
MDA-MB-231
Relative
red intensity (%)
shGFP
shBMI1
**
**
**
**

Itou Fig. 5

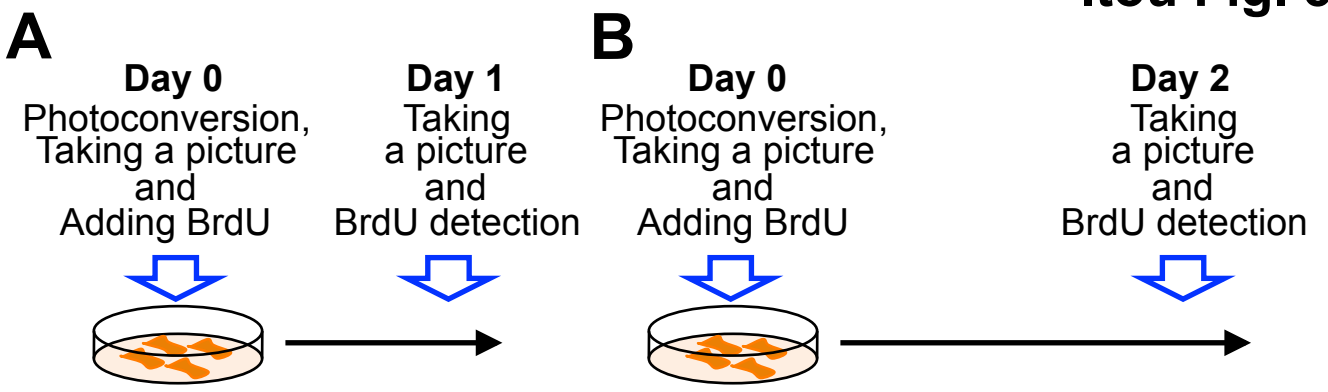
A
Day 0
Photoconversion,
Taking a picture
and
Adding BrdU
Day 1
Taking
a picture
and
BrdU detection
B
Day 0
Photoconversion,
Taking a picture
and
Adding BrdU
Day 2
Taking
a picture
and
BrdU detection

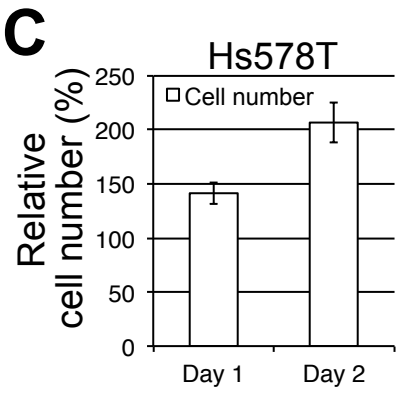
C
Hs578T
Cell number
Relative cell number (%)
250
200
150
100
50
0
Day 1
Day 2

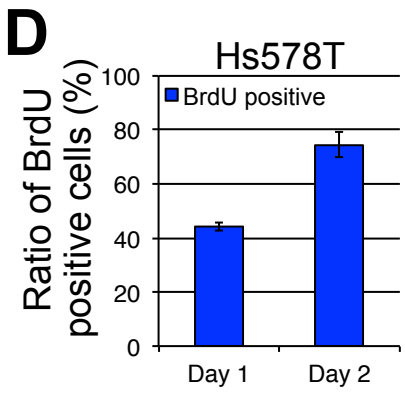
D
Hs578T
BrdU positive
Ratio of BrdU positive cells (%)
100
80
60
40
20
0
Day 1
Day 2

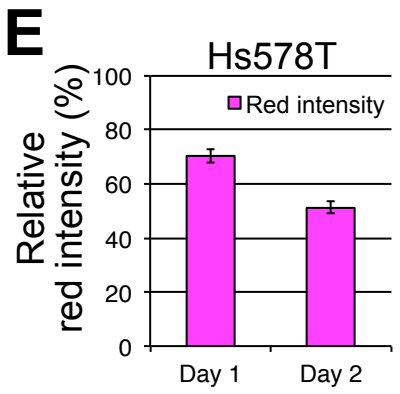
E
Hs578T
Red intensity
Relative red intensity (%)
100
80
60
40
20
0
Day 1
Day 2

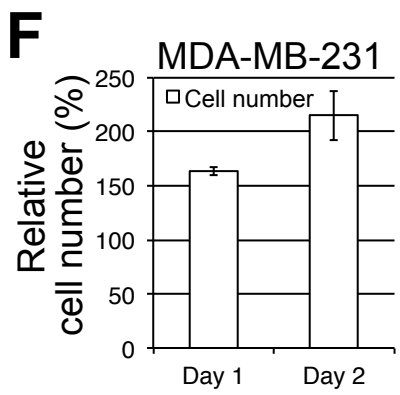
F
MDA-MB-231
Cell number
Relative cell number (%)
250
200
150
100
50
0
Day 1
Day 2

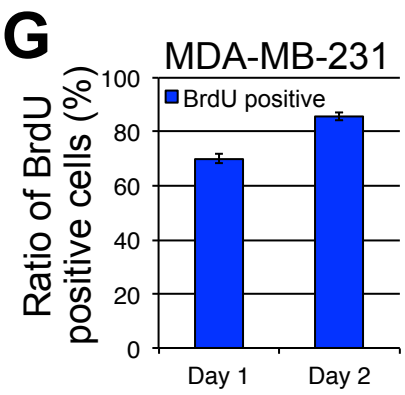
G
MDA-MB-231
BrdU positive
Ratio of BrdU positive cells (%)
100
80
60
40
20
0
Day 1
Day 2

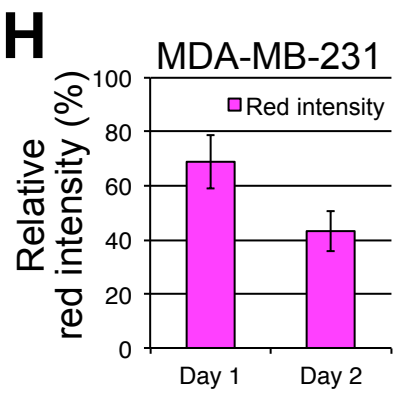
H
MDA-MB-231
Red intensity
Relative red intensity (%)
100
80
60
40
20
0
Day 1
Day 2

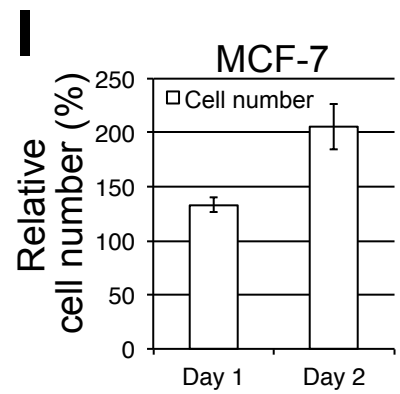
I
MCF-7
Cell number
Relative cell number (%)
250
200
150
100
50
0
Day 1
Day 2

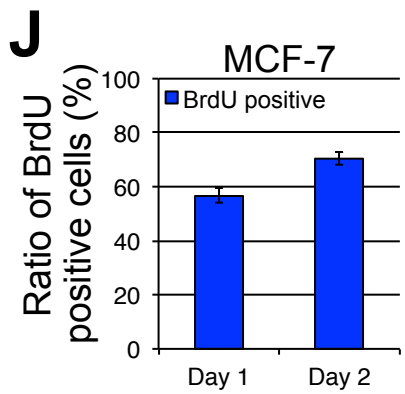
J
MCF-7
BrdU positive
Ratio of BrdU positive cells (%)
100
80
60
40
20
0
Day 1
Day 2

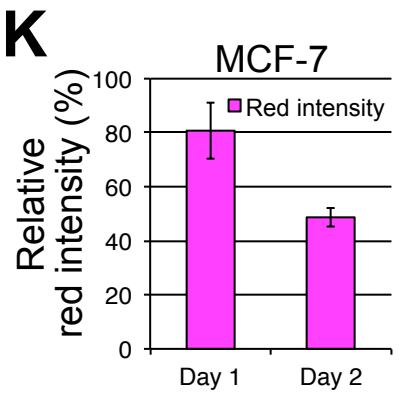
K
MCF-7
Red intensity
Relative red intensity (%)
100
80
60
40
20
0
Day 1
Day 2

Itou Fig. 6

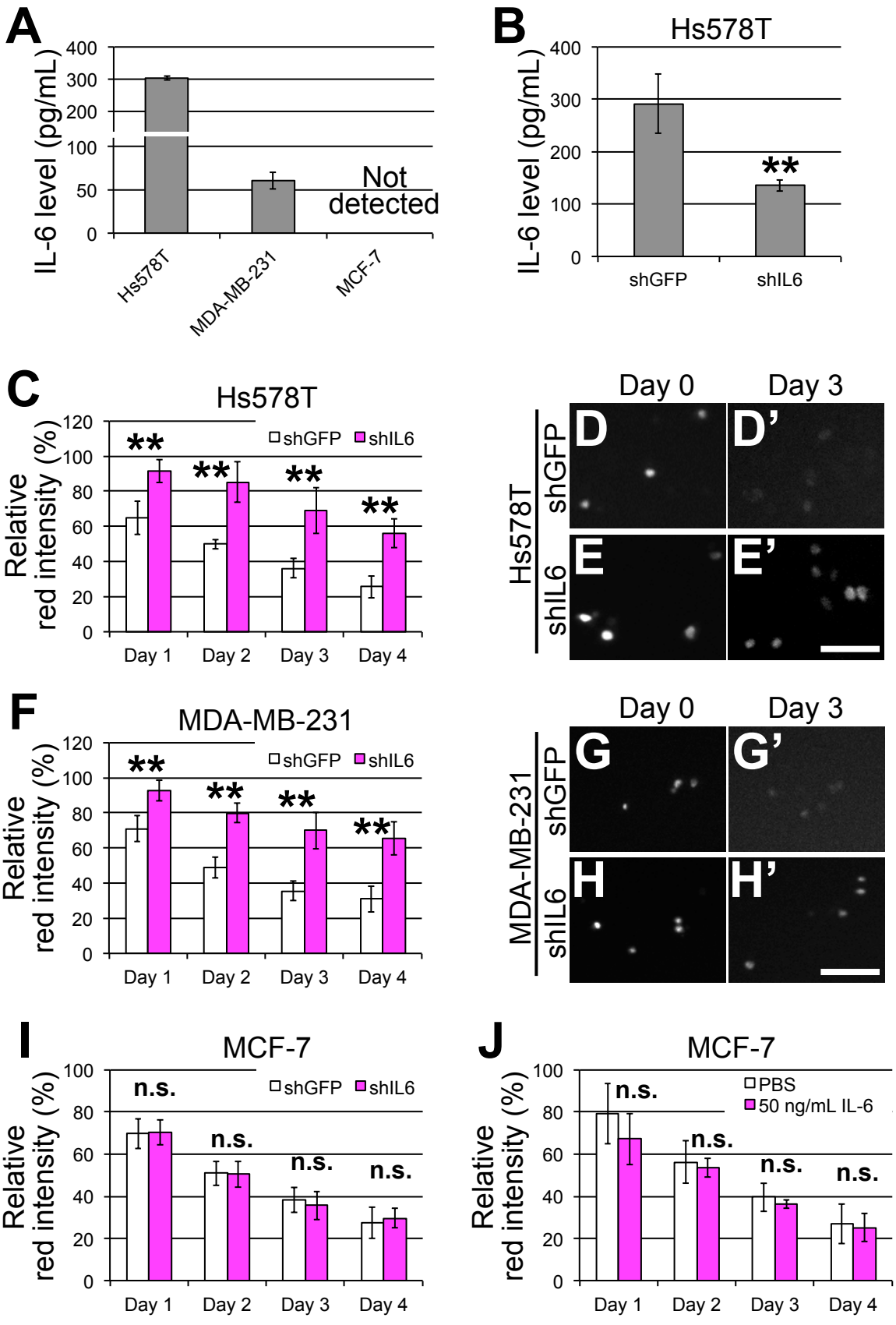
A
IL-6 level (pg/mL)
400
300
200
100
50
0
Not detected
Hs578T
MDA-MB-231
MCF-7
B
Hs578T
IL-6 level (pg/mL)
400
300
200
100
0
**
shGFP
shIL6
C
Hs578T
Relative red intensity (%)
120
100
80
60
40
20
0
shGFP
shIL6
**
Day 1
Day 2
Day 3
Day 4
Day 0
Day 3
Hs578T
shGFP
shIL6
D
D'
E
E'
F
MDA-MB-231
Relative red intensity (%)
shGFP
shIL6
**
Day 1
Day 2
Day 3
Day 4
Day 0
Day 3
MDA-MB-231
shGFP
shIL6
G
G'
H
H'
I
MCF-7
Relative red intensity (%)
100
80
60
40
20
0
shGFP
shIL6
n.s.
Day 1
Day 2
Day 3
Day 4
J
MCF-7
Relative red intensity (%)
PBS
50 ng/mL IL-6
n.s.
Day 1
Day 2
Day 3
Day 4

Itou Fig. 7

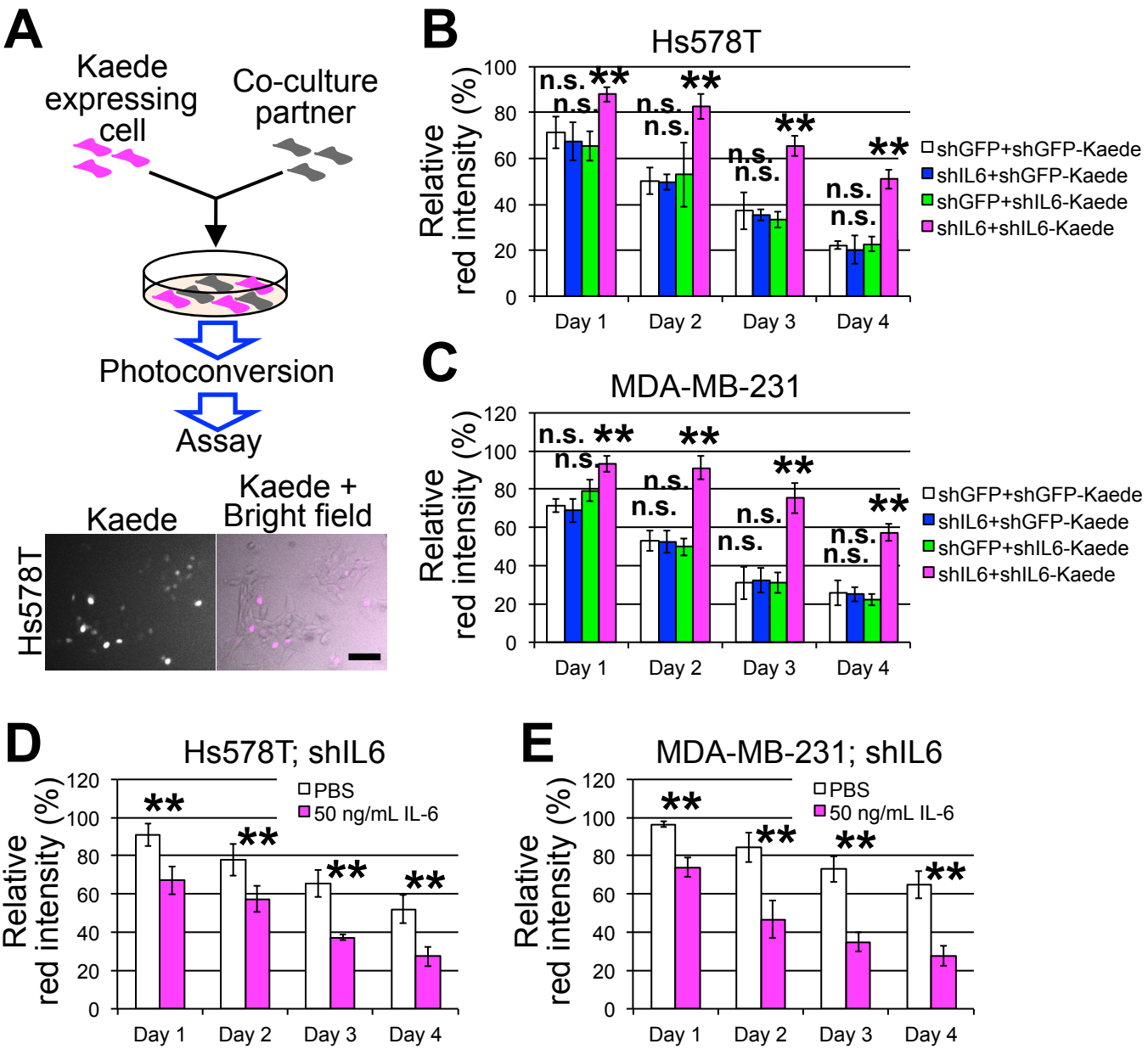
A
Kaede expressing cell
Co-culture partner
Photoconversion
Assay
Kaede
Kaede + Bright field
Hs578T
B
Hs578T
Relative red intensity (%)
Day 1
Day 2
Day 3
Day 4
shGFP+shGFP-Kaede
shIL6+shGFP-Kaede
shGFP+shIL6-Kaede
shIL6+shIL6-Kaede
C
MDA-MB-231
D
Hs578T; shIL6
PBS
50 ng/mL IL-6
E
MDA-MB-231; shIL6

Itou Fig. 8

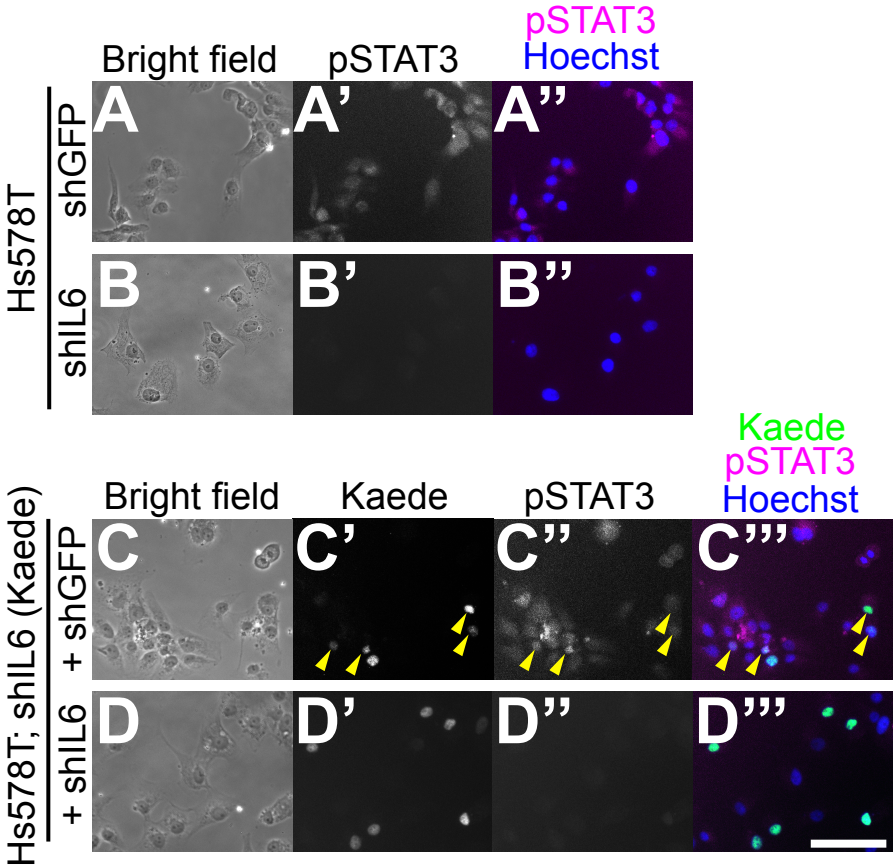
Bright field
pSTAT3
pSTAT3
Hoechst
Hs578T
shGFP
shIL6
A
A'
A''
B
B'
B''
Kaede
pSTAT3
Hoechst
Bright field
Kaede
pSTAT3
Hs578T; shIL6 (Kaede)
+ shGFP
+ shIL6
C
C'
C''
C'''
D
D'
D''
D'''

An optical labeling-based proliferation assay system reveals the paracrine effect of interleukin-6 in breast cancer

Junji Itou, Sunao Tanaka, Fumiaki Sato, Ryutaro Akiyama, Yasuhiko Kawakami and Masakazu Toi

Supplementary data

- Supplementary figure, Fig. S1
- Supplementary figure, Fig. S2
- Supplementary figure, Fig. S3
- Supplementary figure, Fig. S4
- Supplementary figure, Fig. S5
- Supplementary figure, Fig. S6
- Supplementary figure, Fig. S7
- Supplementary Table S1
- Supplementary Table S2
- Supplementary Table S3
- Movie

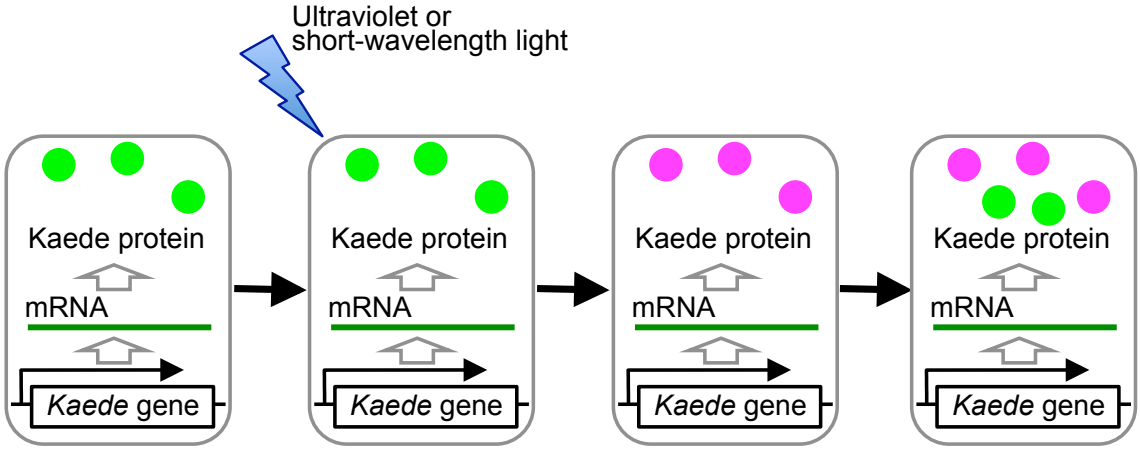

Fig. S1. Photoconverted Kaede is generated by light irradiation. When the cells are exposed to strong ultraviolet or short wavelength light, the fluorescence of Kaede changes to red. Because newly synthesized Kaede fluoresces green, Kaede-red intensity does not increase unless cells are re-exposed to strong light.

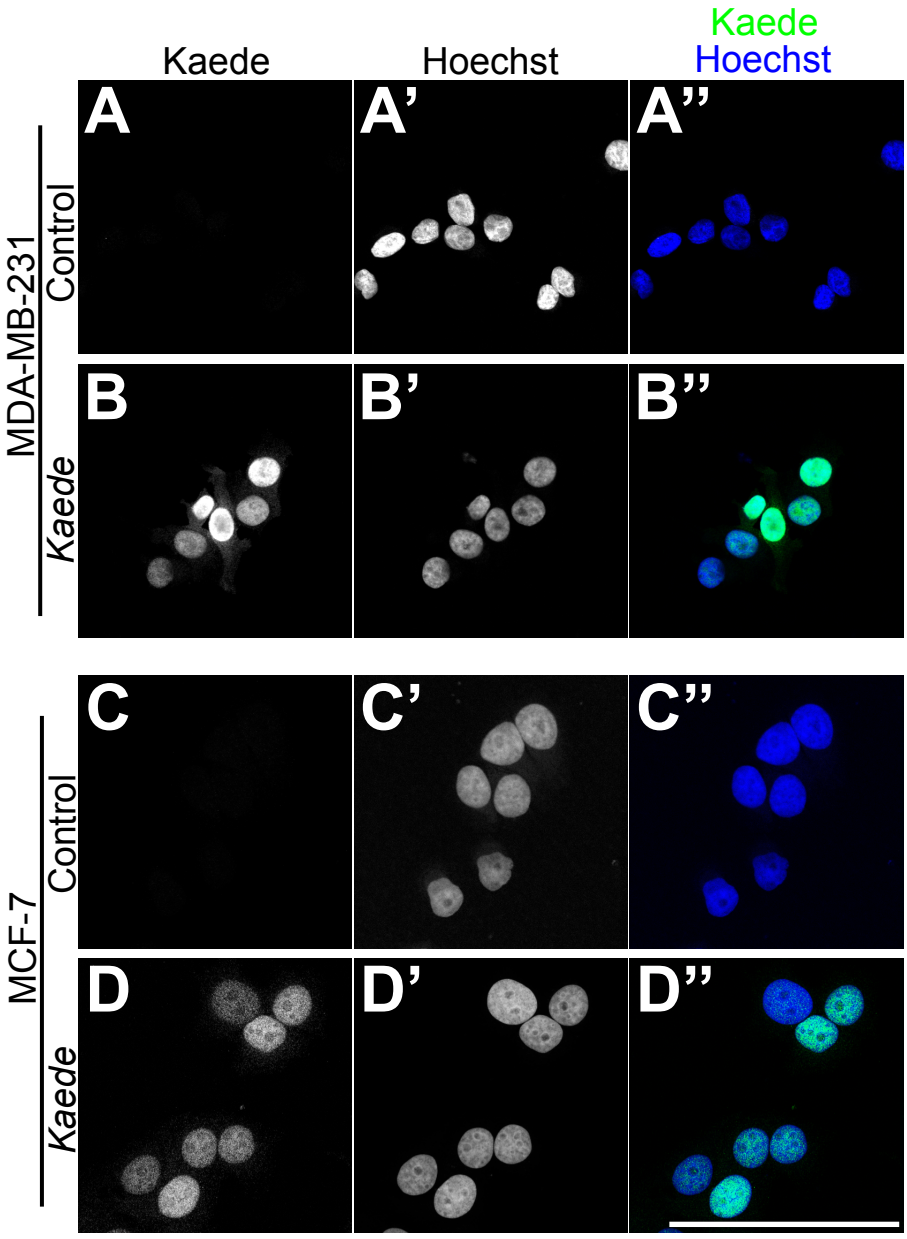

Fig. S2. Nuclear localization of Kaede molecules. The Kaede signal was detected with an anti-FLAG antibody in the unlabeled controls (A,C), and in Kaede-labeled cells (B,D). Representative confocal images are shown. MDA-MB-231 (A,B, $n = 3$ rounds of staining) and MCF-7 cells (C,D, $n = 3$ rounds of staining) were used. A', B', C', and D' show nuclear staining by Hoechst 33342. A'', B'', C'', and D'' show the merged images. Bars indicate 100 μm.

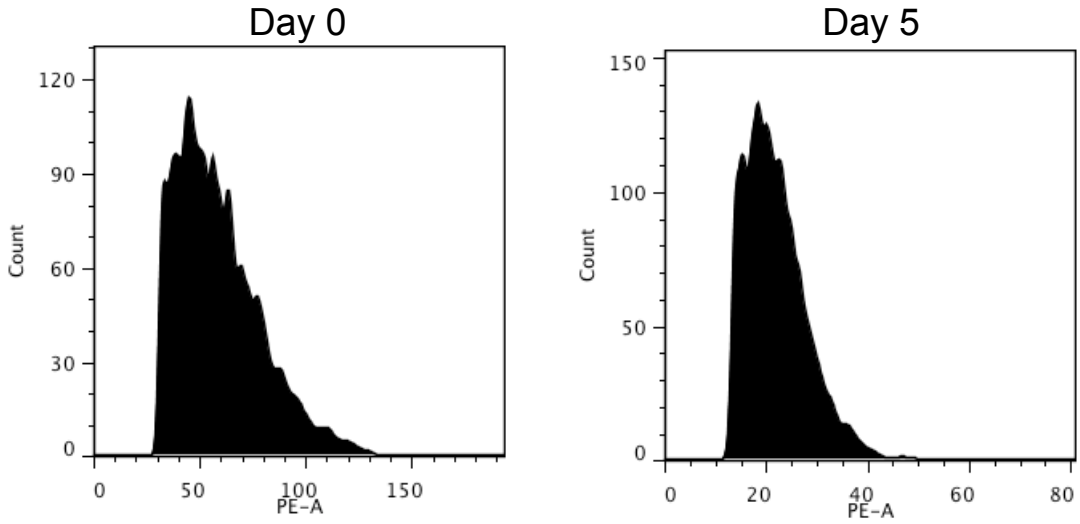

Fig. S3. Distribution of Kaede-red intensity. The histograms show the representative tight distribution of Kaede-red-positive MDA-MB-231 cells observed via flow cytometry.

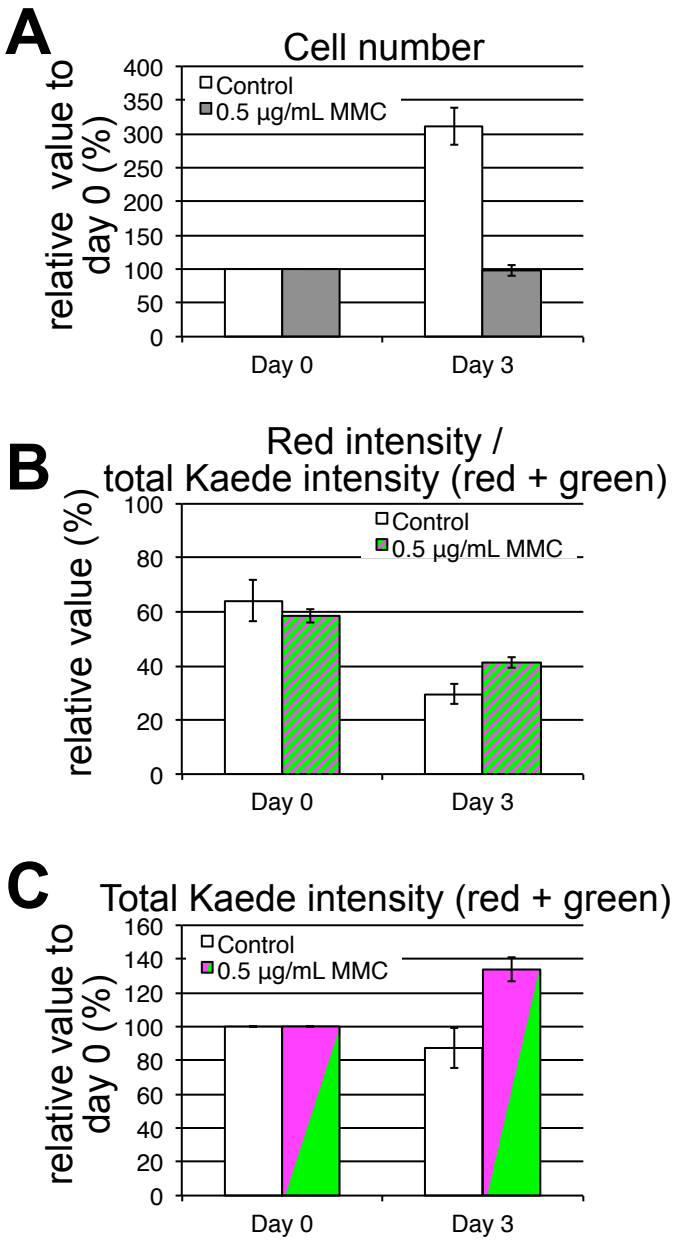

Fig. S4. Comparison of red intensity to total Kaede intensity. Graphs show the change in cell number (A), red intensity/total Kaede intensity (B), and total Kaede intensity (C). Data were obtained from the same cultures analyzed in Fig. 3D.

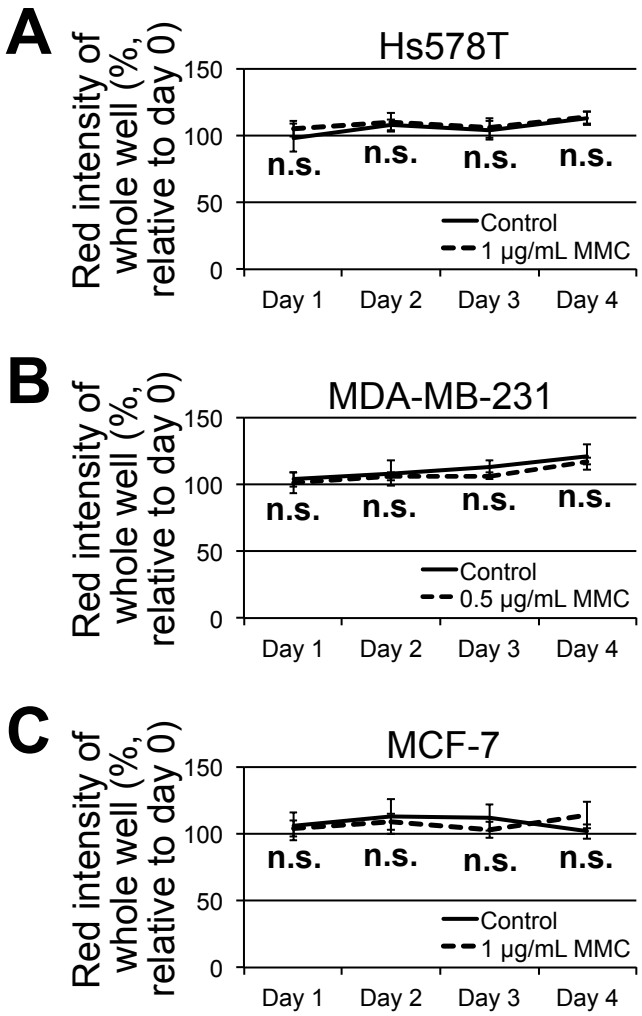

Fig. S5. Total red intensity did not decrease during analysis. The total red intensity of a group of cells was measured in Hs578T (A, $n = 4$), MDA-MB-231 (B, $n = 4$), and MCF-7 cells (C, $n = 4$). Values relative to day 0 were graphed. The total intensity of Kaede-red did not differ significantly between proliferating (control) and growth-inhibited (MMC) cells. Student's *t*-test was used for statistical analysis. n.s.: non-significant change. Error bars represent the standard deviation.

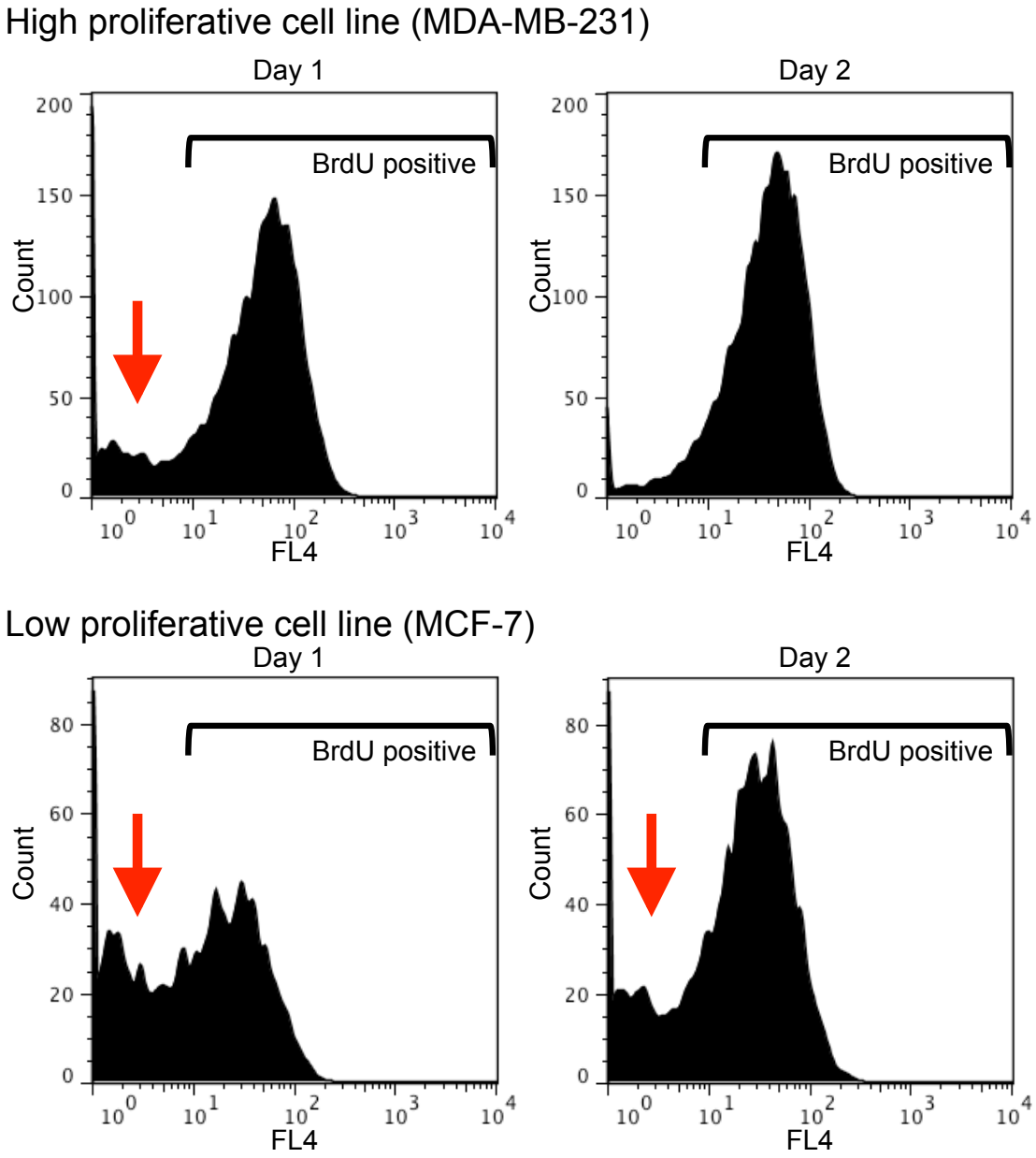

Fig. S6. Change oh BrdU positive and negative populations. The histograms show the representative distribution of BrdU signals observed via flow cytometry. BrdU negative population was observed (red arrow).

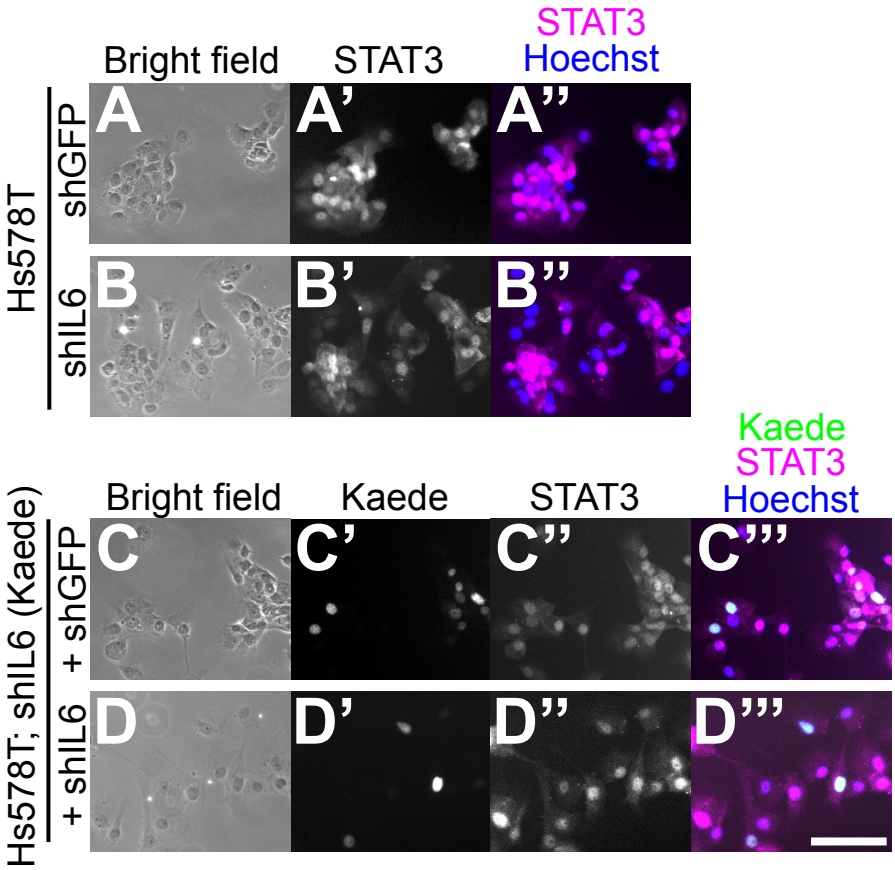

Fig. S7. No change in STAT3 levels in shIL6-expressing cells. (A,B) STAT3 was detected in shGFP- (A) and shIL6-expressing Hs578T cells (B), and STAT3 levels did not change. (C,D) STAT3 level in shIL6-expressing Kaede cells co-cultured with shGFP- (C) or shIL6-expressing cells (D). Bar indicates 100 μm.

Table S1. TUNEL-positive cell numbers in irradiated samples

	Hs578T		MDA-MB-231		MCF-7	
	Total	TUNEL	Total	TUNEL	Total[1]	TUNEL
No irradiation[1]	1,500	20	2,390	15	1,305	31
340-380 nm light[2]	2,008	24	2,667	26	1,624	39
Ultraviolet[3]	1,237	157	1,041	69	1,225	91

1. Cell number from 3 analyses of Hs578T and MDA-MB-231 cells, and 4 analyses of MCF-7 cells.

2. Cell number from 3 analyses of Hs578T and MCF-7 cells, and 4 analyses of MDA-MB-231 cells.

3. Cell number from 5 analyses of Hs578T cells, 3 analyses of MDA-MB-231 cells, and 4 analyses of MCF-7 cells.

Table S2. Nucleus size of breast cancer cell lines[1]

	Hs578T (μm^2)	MDA-MB-231 (μm^2)	MCF-7 (μm^2)
Mean	297.46	108.13	166.58
s.d.[2]	10.50 (3.52%)	5.02 (4.64%)	8.55 (5.13%)
Maximum	314.99	116.18	185.90
Minimum	276.26	98.11	154.91

1. One hundred cells were analyzed per cell line.

2. s.d.: standard deviation

Table S3. Red intensity after cell division relative to before division[1]

	Hs578T (%)	MDA-MB-231 (%)	MCF-7 (%)
Mean	51.54	52.79	52.33
s.d.[2]	8.87	10.32	9.09
Maximum	76.92	77.48	77.89
Minimum	35.34	27.38	28.57

1. Fifty divisions (100 daughter cells) were analyzed.

2. s.d.: standard deviation

Movie. Reduction in Kaede-red fluorescence per cell during proliferation. Kaede-expressing cells were photoconverted and set on the stage of a confocal microscope. Time-lapse images were taken every 10 min. Red intensity decreased following cell division.